Article

Satellite-Observed Variations and Trends in Carbon Monoxide over Asia and Their Sensitivities to Biomass Burning

Xun Zhang [1], Jane Liu [2,3,]* , Han Han [2], Yongguang Zhang [1] , Zhe Jiang [4], Haikun Wang [2], Lingyun Meng [2], Yi Chen Li [2] and Yi Liu [2]

[1] International Institute for Earth System Science, Nanjing University, Nanjing 210023, China; DG1727037@smail.nju.edu.cn (X.Z.); yongguang_zhang@nju.edu.cn (Y.Z.)
[2] School of Atmospheric Sciences, Nanjing University, Nanjing 210023, China; DG1728004@smail.nju.edu.cn (H.H.); wanghk@nju.edu.cn (H.W.); 141170037@smail.nju.edu.cn (L.M.); MG1728042@smail.nju.edu.cn (Y.C.L.); MG1928043@smail.nju.edu.cn (Y.L.)
[3] Department of Geography and Planning, University of Toronto, Ontario M5S 3G3, Canada
[4] School of Earth and Space Sciences, University of Science and Technology of China, Hefei 230026, China; zhejiang@ustc.edu.cn
* Correspondence: janejj.liu@utoronto.ca

check for updates

Abstract: As the carbon monoxide (CO) total column over Asia is among the highest in the world, it is important to characterize its variations in space and time. Using Measurements of Pollution in the Troposphere (MOPITT) and Atmospheric InfraRed Sounder (AIRS) satellite data, the variations and trends in CO total column over Asia and its seven subregions during 2003–2017 are investigated in this study. The CO total column in Asia is higher in spring and winter than in summer and autumn. The seasonal maximum and minimum are in spring and summer respectively in the regional mean over Asia, varying between land and oceans, as well as among the subregions. The CO total column in Asia shows strong interannual variation, with a regional mean coefficient of variation of 5.8% in MOPITT data. From 2003 to 2017, the annual mean of CO total column over Asia decreased significantly at a rate of (0.58 ± 0.15)% per year (or $-(0.11 \pm 0.03) \times 10^{17}$ molecules cm^{-2} per year) in MOPITT data, resulting from significant CO decreases in winter, summer, and spring. In most of the subregions, significant decreasing trends in CO total column are also observed, more obviously over areas with high CO total column, including eastern regions of China and the Sichuan Basin. The regional decreasing trends in these areas are over 1% per year. Over the entire Asia, and in fire-prone subregions including South Siberia, Indo-China Peninsula, and Indonesia, we found significant correlations between the MOPITT CO total column and the fire counts from the Moderate Resolution Imaging Spectroradiometer (MODIS). The variations in MODIS fire counts may explain 58%, 60%, 36%, and 71% of the interannual variation in CO total column in Asia and these three subregions, respectively. Over different land cover types, the variations in biomass burning may explain 62%, 52%, and 31% of the interannual variation in CO total column, respectively, over the forest, grassland, and shrubland in Asia. Extremes in CO total column in Asia can be largely explained by the extreme fire events, such as the fires over Siberia in 2003 and 2012 and over Indonesia in 2006 and 2015. The significant decreasing trends in MODIS fire counts inside and outside Asia suggest that global biomass burning may be a driver for the decreasing trend in CO total column in Asia, especially in spring. In general, the variations and trends in CO total column over Asia detected by AIRS are similar to but smaller than those by MOPITT. The two datasets show similar spatial and temporal variations in CO total column over Asia, with correlation coefficients of 0.86–0.98 in the annual means. This study shows that the interannual variation in atmospheric CO in Asia is sensitive to biomass burning, while the decreasing trend in atmospheric CO over Asia coincides with the decreasing trend in MODIS fire counts from 2003 to 2017.

1. Introduction

Atmospheric carbon monoxide (CO) plays an important role in the atmospheric chemistry, serving as a precursor of ozone [1]. CO is a major air pollutant, harmful to human health. It is the third most abundant carbon species, being linked to global carbon cycle [2,3]. With the atmospheric lifetime of about weeks to months, CO is a good tracer of air pollution [4,5]. Therefore, it is important to identify the spatial patterns, temporal variations, and long-term trends in atmospheric CO concentrations.

Since 2000, satellite instruments have provided global and long-term records of atmospheric CO [6–8]. Satellite measurements have been used in characterizing the spatial distribution, temporal variations, and transport processes of atmospheric CO [3,9–11]. Using well-validated satellite measurements, including Measurements of Pollution in the Troposphere (MOPITT) and Atmospheric InfraRed Sounder (AIRS), previous studies have shown that atmospheric CO is quite higher in Asia than in other continents [12]. Influenced by emissions, meteorology and chemistry, atmospheric CO concentrations in Asia vary seasonally and interannually [13,14]. Atmospheric CO concentrations in Asia have different seasonalities over different subregions and vertical layers [15–17]. Bai et al. [18] showed that CO total column over China peaks in spring. Girach and Nair [15] showed that CO concentrations in the lower troposphere over India peak in winter.

Based on satellite data, previous studies characterized the global and regional trends in atmospheric CO [19,20]. On global scale, a significant decreasing trend during 2000–2012 in CO total column was reported [19], which agrees with the situ observations, aircraft measurements, and numerical simulations [17,21,22]. Some studies explored the CO trends in subregions of Asia [16,19,23]. Zheng et al. [24] stated that regional mean CO total column in South Asia showed a significant increasing trend during 2000–2017, while Yin and Wang et al. [25] reported no significant decreasing trend in Southeast Asia during 2001–2016. Up to today, there are few studies specifically focused on the spatial and temporal variations and trends in CO over Asia, so a comprehensive investigation to address the issues is needed.

Global CO sources are mainly from anthropogenic activities (500–600 Tg yr^{-1}) and biomass burning (300–600 Tg yr^{-1}), which have significant year-to-year variations [26,27]. Biomass burning alone can impact the seasonality and interannual variations in global CO concentrations [24]. On regional scale, the influence of biomass burning is also important in Africa [28,29], South America [9,30], Northwest America [31], East Asia [32–34], Southeast Asia [25], Australia [35] and Russia [36,37]. Asia is one of the continents with strong biomass burning [38]. Biomass burning in Asia is mainly in the form of forest fires and crop residue burning. The amount of fires is highest in Southeast Asia, followed by East Asia and South Asia [39]. Worden et al. [40] and Nechita-Banda et al. [41] reported the strong fire events in Indonesia in 2006 and 2015, showing that CO emissions from the fires greatly enhanced atmospheric CO abundances. Although previous studies have emphasized the importance of biomass burning to atmospheric CO abundances in Asia, few of them have explored the influences of biomass burning on the interannual variation and trends in CO over Asia in a long period.

Up to now, our understanding of the CO variation and trend over Asia and underlying mechanisms for the variation and trend is still limited. To fill the research gaps mentioned above, the first objective of this study is to characterize (i) the spatial and temporal variations in CO in Asia, with emphasis on the interannual variation, and (ii) the trends in CO concentrations over 2003–2017 in Asia and its subregions (Section 3). The second objective is to explore influences of biomass burning on the interannual variation and the long-term trends in CO over Asia from 2003–2017 (Section 4). MOPITT and AIRS satellite data are used because of their long-term records, high spatial coverage,

and good quality. In Section 2, we introduce satellite and fire data. Discussion and conclusions are provided in Sections 4 and 5, respectively.

2. Data and Methods

2.1. Study Area, Study Period, and Statistics Analysis

Asia (10°S–60°N, 60°E–140°E) is the domains of interest in this study. The study period is from 2003 to 2017. Since Asia is large and nonhomogeneous, we assessed variations and trends in CO total column over Asia and its subregions, including South Siberia (50°N–60°N, 60°E–140°E), India (5°N–32°N, 70°E–88°E), Indo-China Peninsula (10°N–22°N, 88°E–110°E), Indonesia (3°S–3°N, 95°E–115°E), the Sichuan Basin (27°N–33°N, 102°E–110°E), North China (32°N–42°N, 110°E–125°E), and South China (22°N–32°N, 110°E–122°E) (Figure 1a). The seasons are defined as: spring (March–May), summer (June–August), autumn (September–November), and winter (December–February). The trends are quantified using the simple linear regression. The slope of the linear fit represents the increasing or decreasing rate of CO. In this study, the statistics are reported as significant when $p < 0.05$.

2.2. Satellite Carbon Monoxide Data and Analysis

MOPITT (https://terra.nasa.gov/about/terra-instruments/mopitt) is an instrument on board the National Aeronautics and Space Administration (NASA) Earth Observing System Terra spacecraft launched in 1999, using near-infrared at 2.3 μm and thermal-infrared radiation at 4.7 μm. MOPITT detects CO at a spatial resolution of 22 km × 22 km at nadir. MOPITT monthly products (MOP03JM, level 3, version 7) with a horizontal resolution of 1° × 1° (latitude × longitude) were used [42]. To enhance data quality, the daytime data with the degree of freedom for signal higher than 0.75 were selected.

CO data from AIRS instrument (https://airs.jpl.nasa.gov/mission_and_instrument/overview) were analyzed as a supplement. AIRS is on board Aqua, launched in 2002 by NASA. AIRS resolving power is $\lambda/\Delta\lambda = 1200$, resulting in a spectral resolution ~1.8 cm^{-1} for the 4.6 μm CO absorption. AIRS provides twice daily and near-global coverage of tropospheric CO [43]. AIRS version 6 products (AIRS3STM and AIRS3SPM) of monthly CO data at 1° × 1° were used. Similar to the data filtering for MOPITT measurements, AIRS daytime CO data with the degree of freedom for signal higher than 0.5 were selected.

Both MOPITT [6,7] and AIRS [8] are most sensitive to CO in the middle troposphere. Deeter et al. [7] suggested that compared with the in situ observations from National Oceanic and Atmospheric Administration (NOAA) validation sites, CO total column from MOPITT version 7 product has a correlation coefficient of 0.93 and a bias of 0.3×10^{17} molecules cm^{-2}. McMillan et al. [44] suggested that compared with in the situ CO profiles, AIRS version 5 retrievals at 300–900 hPa are biased by 6–10% in the northern mid-latitudes. MOPITT and AIRS CO data have been widely used in investigating the distribution, transport, sources, and sinks of global tropospheric CO [20,45].

### 2.3. Fire Count and Emission Data and Land Cover Data

To fit the horizontal resolution of satellite CO data, we gridded the Moderate Resolution Imaging Spectroradiometer (MODIS) monthly active fire count data (MCD14ML) [46] into 1° × 1° (latitude × longitude) globally from 2003 to 2017. The data with the confidence level higher than 0.75 were selected. The Global Fire Emissions Database (GFED) is a bottom-up inventory for fire emissions based on satellite burned areas [47]. The version GFED 4.1s data [27] were used, including small fires with the spatial resolution of 0.25° × 0.25° during 2003–2017. We regridded the CO emission data from biomass burning into 1° × 1° (latitude × longitude) globally from 2003–2017.
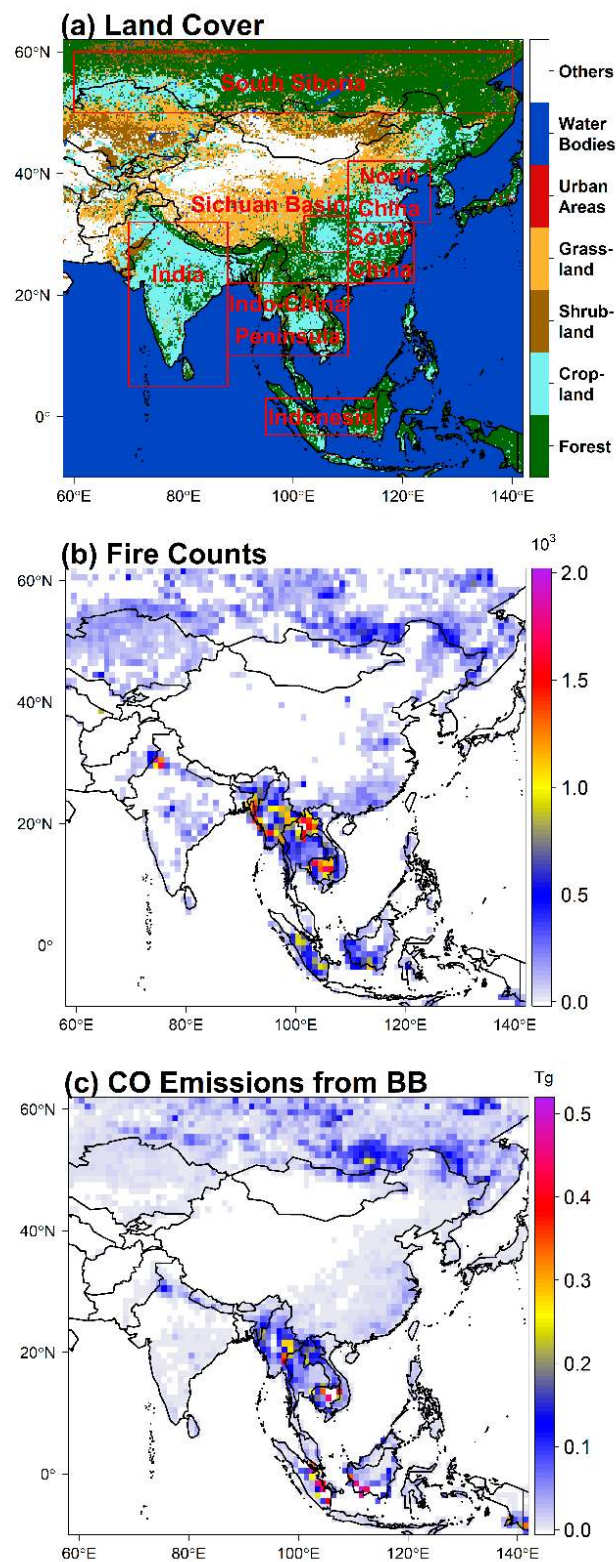
Figure 1. (**a**) Land cover types over Asia in 2015. The boxed areas indicate the subregions, namely, South Siberia, India, Indo-China Peninsula, Indonesia, the Sichuan Basin, North China, and South China. (**b**) The annual total fire counts from the Moderate Resolution Imaging Spectroradiometer (MODIS) data [46] and (**c**) the annual total carbon monoxide (CO) emissions from biomass burning (BB) from the Global Fire Emissions Database (GFED) data [27]. The grid size is $1° \times 1°$. The values in (**b**) and (**c**) are the means over 2003–2017.

The land cover data from the European Space Agency Climate Change Initiative (ESA CCI) with a resolution of 300 m were used. The land cover data are updated every year and available from 2003 to 2015. As the land cover data in 2016 and 2017 were not available, the land cover in 2015 was used as a substitute. We regridded the original ESA CCI land cover data to grids of $1° \times 1°$ (Figure 1a). The most dominant land cover type in each of the grids of $1° \times 1°$ is assigned to that grid. The original 37 classes of land cover types were reclassified to the seven land cover types: forest, cropland, shrubland, grassland, urban areas, water bodies and others as shown in Figure 1a. Reclassified land cover types is listed in detail in Supplement as Table S1. MODIS fire count data and ESA CCI land cover data were widely used and have been well validated in previous studies [46].

Figure 1b shows the spatial distribution of the annual total fire counts over Asia, averaged over 2003–2017. Fires occur more in the Indo-China Peninsula, Indonesia, and South Siberia than in other subregions in Asia. The three fire-prone subregions contribute a majority of CO fire emissions in Asia (Figure 1c) [48–50]. The three regions are covered mostly by forest and cropland (Figure 1a). Among seasons, fires occur over the Indo-China Peninsula mostly in spring and winter, over Indonesia mostly in summer and autumn, and over South Siberia mostly in spring and summer (Figure 2). Dry and hot climate in spring, summer and autumn is the main reason for strong fires in Indo-China Peninsula, Indonesia, and South Siberia [51,52]. In winter, since the cold Siberian high and the East Asian winter monsoon can bring frequent and severe cold surges and/or snowstorms, leading to the surface air temperature below the point of fire ignition [53,54]. Therefore, fires are inactive in winter over South Siberia and latitudes above 23°N. In the annual mean, CO emissions from biomass burning in Asia are ~76.5 Tg during 2003–2017 (Figure 3b), which account for 23% of the global fire emissions (332.5 Tg). Forest contributes approximately 59% of the CO emissions from biomass burning (Figure 3d) annually. Seasonally, the estimated fire CO emissions in Asia rank as 25.6 Tg in spring, >23.7 Tg in autumn, >17.9 Tg in summer, >8.6 Tg in winter.
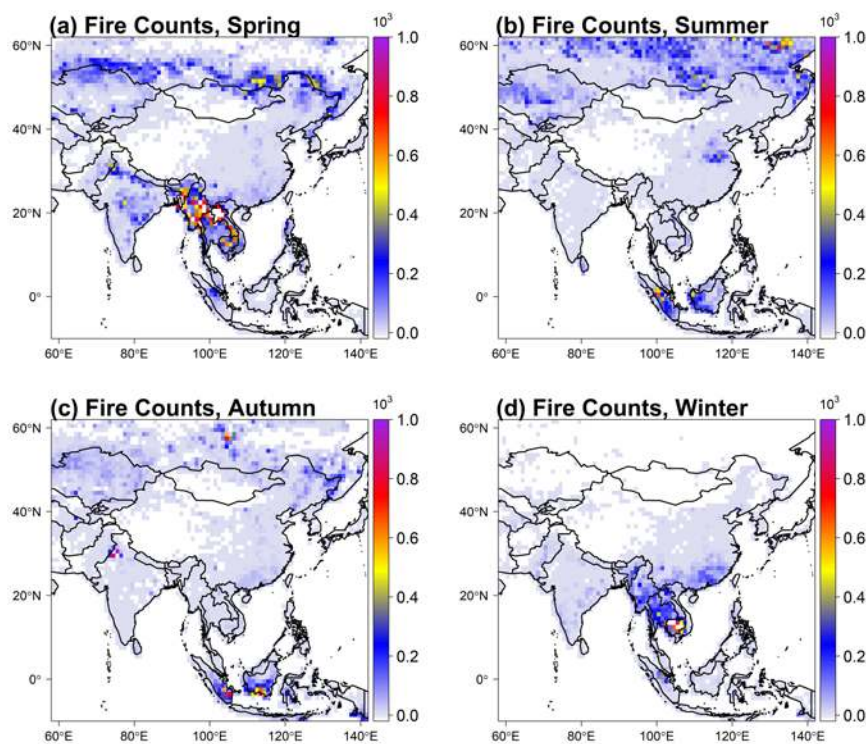
Figure 2. Spatial distributions of the seasonal total fire counts in (**a**) spring, (**b**) summer, (**c**) autumn and (**d**) winter from the MODIS data [46]. The values are the mean over 2003–2017. The grid size is $1° \times 1°$.
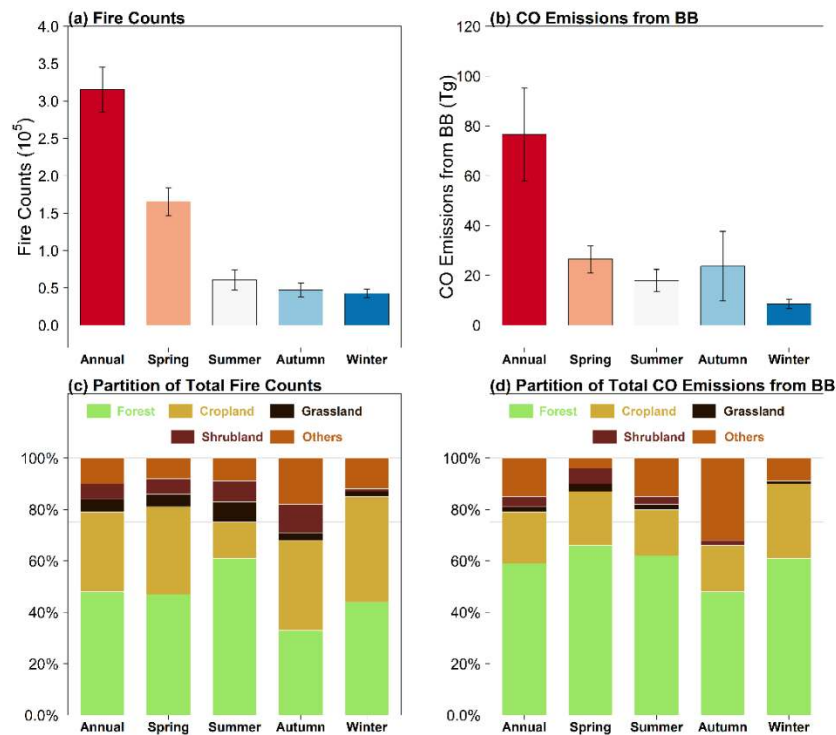
Figure 3. (**a**) MODIS total fire counts and (**b**) GFED4 total CO emissions from biomass burning (BB). The fractional contribution of each land cover type to the total fire counts (**c**) and to the total CO emissions from BB (**d**). The bars in (**a**) and (**b**) indicate the standard deviation. All the values are the means over 2003–2017.

3. Results

3.1. Temporal–Spatial Variations and Trends in Atmospheric Carbon Monoxide over Asia

3.1.1. Spatial Variations in Atmospheric Carbon Monoxide over Asia in the Annual Mean and by Season

Figure 4 shows spatial variations in CO total column in Asia in the annual mean and by season from MOPITT and ARIS data averaged over 2003–2017. In the annual mean, CO total columns from MOPITT and AIRS show similar spatial variations over Asia. CO total column is high in North China, South China, the Sichuan Basin, and Indo-China Peninsula, and low in the Tibetan Plateau. CO total column from MOPITT is larger than that from AIRS over the land of Asia (Figures 4b and 5b), but lower than that from AIRS over the ocean (Figures 4c and 5c). The two datasets have a significant correlation over Asia, with the correlation coefficient ranging from 0.76 to 0.98 (Figure 4). The correlation coefficient in the mean over Asia between the two datasets reaches as high as 0.86–0.98 in all seasons (Figure 5). In the annual mean, the regional mean CO total columns over Asia retrieved from MOPITT and AIRS are $(19.3 \pm 4.3) \times 10^{17}$ molecules cm^{-2} and $(18.5 \pm 2.8) \times 10^{17}$ molecules cm^{-2} respectively (Figure 6a). Over the four regions with high CO concentrations: North China, South China, the Sichuan Basin and Indo-China Peninsula, the annual mean CO total column from MOPITT is $(28.1 \pm 4.2) \times 10^{17}$ molecules cm^{-2}, $(27.2 \pm 2.4) \times 10^{17}$ molecules cm^{-2}, $(23.4 \pm 5.2) \times 10^{17}$ molecules cm^{-2}, and $(23.9 \pm 2.7) \times 10^{17}$ molecules cm^{-2}. These values are respectively 7.2×10^{17}, 5.8×10^{17}, 5.1×10^{17}, and 3.1×10^{17} molecules cm^{-2} higher than those from AIRS.
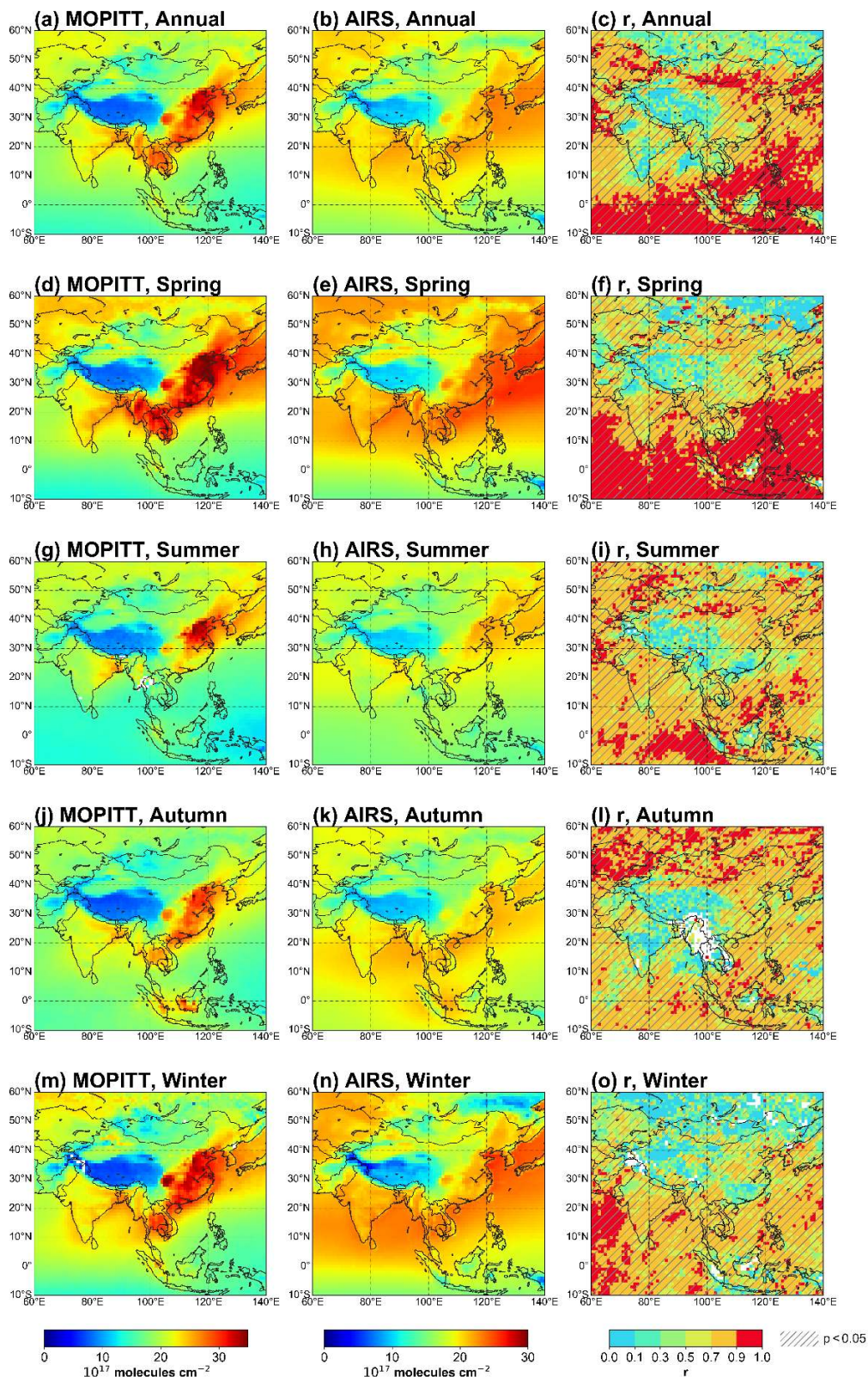
Figure 4. Spatial distributions of annual and seasonal mean CO total columns in Asia averaged over 2003–2017 from the Measurements of Pollution in the Troposphere (MOPITT) (the 1st column) and Atmospheric InfraRed Sounder (AIRS) (the 2nd column). Correlation coefficients (r) between MOPITT and AIRS CO total column (the 3rd column). The shadow areas indicate that the r is statistically significant (p < 0.05). The corresponding annual mean is shown in (**a–c**) (the 1st row). The corresponding seasonal mean is shown in (**d–f**) for spring (the 2nd row), in (**g–i**) for summer (the 3rd row), in (**j–l**) for autumn (the 4th row) and in (**m–o**) for winter (the 5th row).
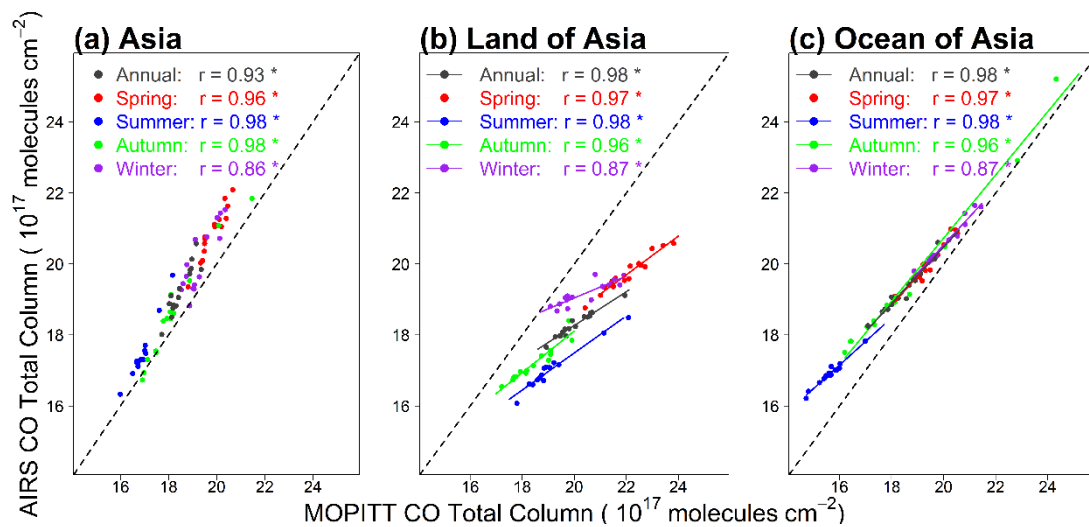
Figure 5. Comparison of CO total column between MOPITT and AIRS data averaged over (**a**) Asia, (**b**) the land of Asia and (**c**) the oceans of Asia, from 2003 to 2017. The correlation coefficients (r) with an asterisk indicate a significance level at over 95% (p < 0.05).

Seasonally (Figure 6), the regional mean CO total column in Asia is higher in spring and winter than in summer and autumn. The seasonal maximum and minimum are in spring and summer over the entire Asia, respectively, varying between land and oceans, as well as among subregions. Over land and in most subregions, the maximum and minimum are in spring and autumn, respectively. However, CO total column over Indonesia peaks in autumn. The seasonality in CO total column is larger over the land than over the oceans in both MOPITT and AIRS data.
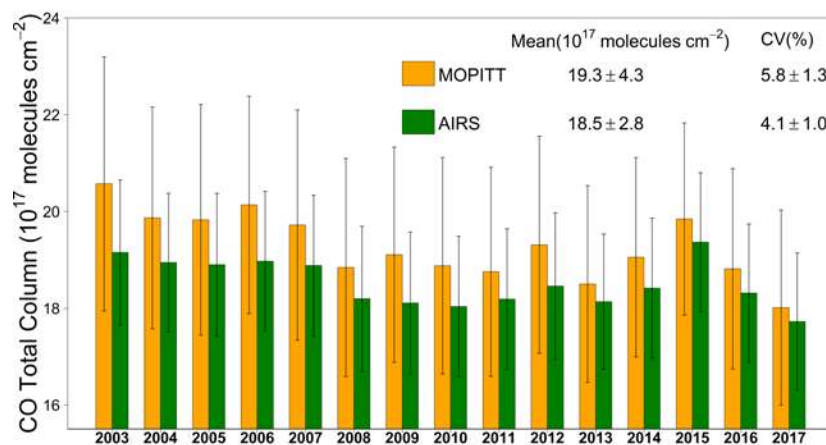
3.1.2. Interannual Variation in Atmospheric Carbon Monoxide over Asia

The interannual variation in CO total column from MOPITT and AIRS over Asia during 2003–2017 are shown in Figure 7. The maximum and minimum in CO total column appeared in 2003 and 2017, respectively. We use the coefficient of variation (CV) as a measure of the strength of the interannual variation in CO total column. CV is the ratio of the standard deviation to the long-term mean. CO total column in Asia shows strong interannual variation, with a regional mean CV of 5.8% in MOPITT data. The mean and CV of CO total column over Asia are both higher in MOPITT than in AIRS data. Spatially, the MOPITT CV in Asia ranges between 1.3% and 37.8% (Figure 8a). CV is generally high in the regions with strong fire activities (Figure 1b,c and Figure 8a) and is highest in Indonesia with the value of 12.7% (Figure 8a,b). CV is also higher over land than over oceans. The Asian mean CV is lower than the global mean CV.
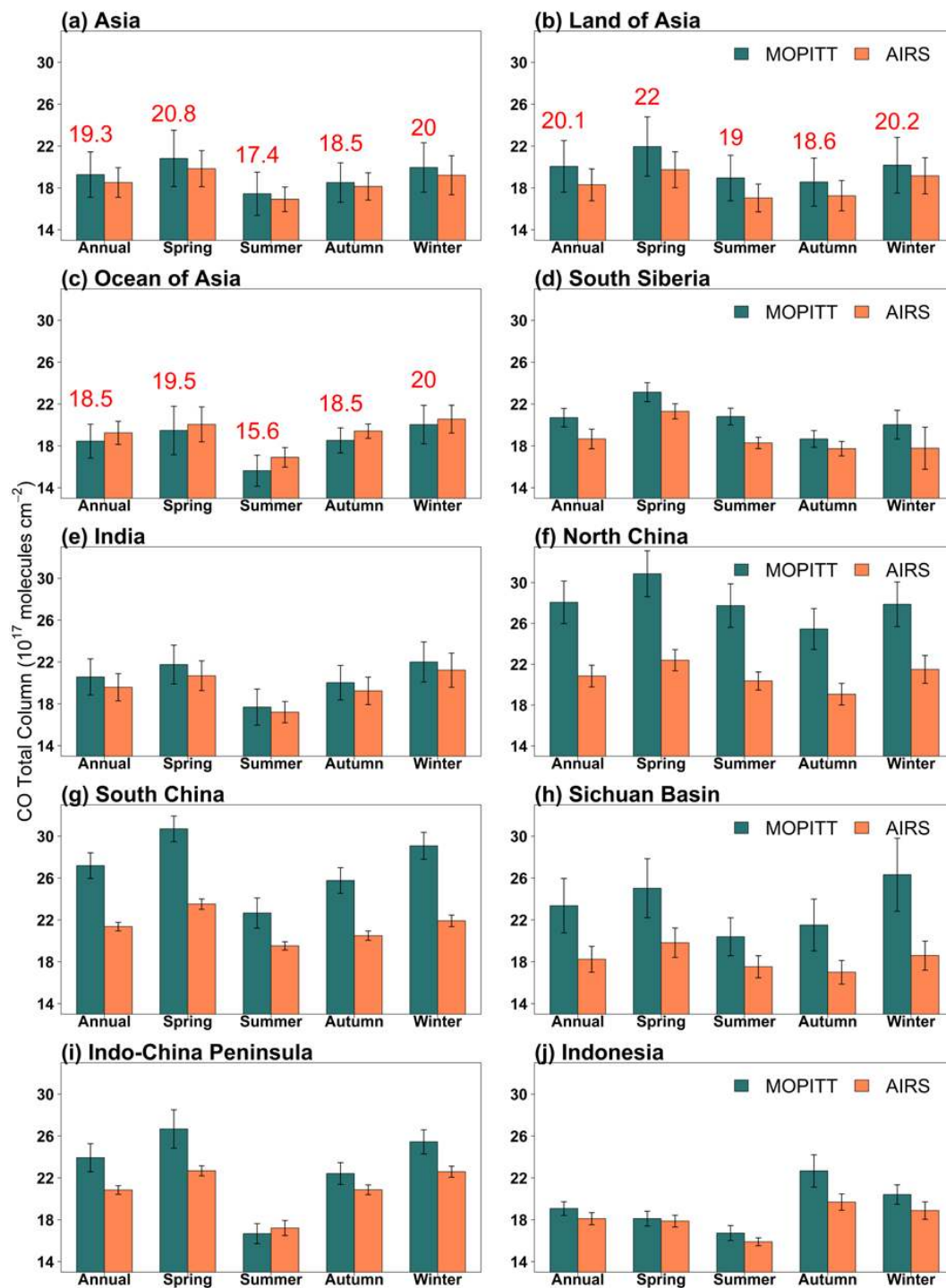
Figure 6. The annual mean and seasonal variations in MOPITT and AIRS CO total columns averaged over Asia and its subregions during 2003–2017: (**a**) Asia, (**b**) the land of Asia, (**c**) the ocean of Asia, (**d**) South Siberia,(**e**) India, (**f**) North China, (**g**) South China, (**h**) the Sichuan Basin, (**i**) Indo-China Peninsula and (**j**) Indonesia. The bar indicates the standard deviation. The values in (**a**), (**b**), and (**c**) are for the mean CO total column from MOPITT data.

Figure 7. Interannual variations in MOPITT and AIRS CO total column averaged over Asia during 2003–2017. The bar indicates the standard deviation. CV is the ratio of the standard deviation to the long-term mean.
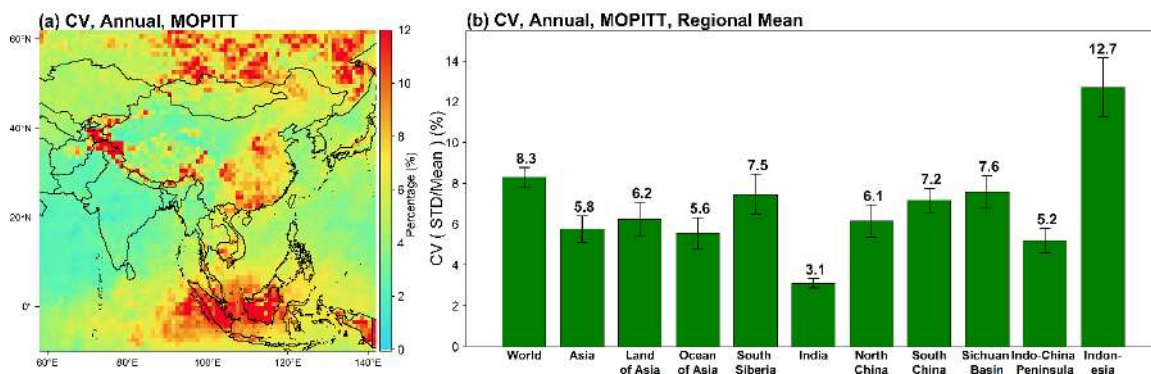

Figure 8. Based on MOPITT data: (**a**) Spatial distribution of CV of the annual CO total column over 2003–2017. (**b**) The means CV of CO total column in Asia, its subregions, and the world. The bar indicates the standard deviation of the mean CV. CV is the ratio of the standard deviation to the long-term mean.

3.1.3. Trends in Atmospheric Carbon Monoxide over Asia from 2003–2017

The trends in the annual mean CO total column derived from MOPITT and AIRS over Asia during 2003–2017 are examined spatially (Figure 9) and on regional mean (Figure 10, Table 1, and Table S2). Both satellite data show that the annual mean CO total column has decreased significantly over large areas of East Asia, including South Siberia, North China, South China, the Sichuan Basin (Figure 9a,b). The decreasing trend in the annual mean CO total column is stronger in Asia than in the world (Table 1). The decreasing trend in the annual mean CO total column is strongest in North China, South China, and the Sichuan Basin where the CO trends range from $-(0.30 \pm 0.04) \times 10^{17}$ molecules cm^{-2} yr^{-1} to $-(0.36 \pm 0.04) \times 10^{17}$ molecules cm^{-2} yr^{-1}. However, no significant trend in the annual mean CO total column is observed over the ocean of Asia, India, Indo-China Peninsula, and Indonesia in MOPITT and AIRS data. The annual mean CO total column in Asia declined at an average rate of 0.58% and 0.30% per year from 2003 to 2017, respectively, in MOPITT and AIRS data (Figure 10a, Table 1, Table S2). The decreasing trend in the annual mean CO total column over Asia is stronger over land in MOPITT data than in AIRS data, but weaker over oceans in MOPITT data than in AIRS data (Figure 10a–c).
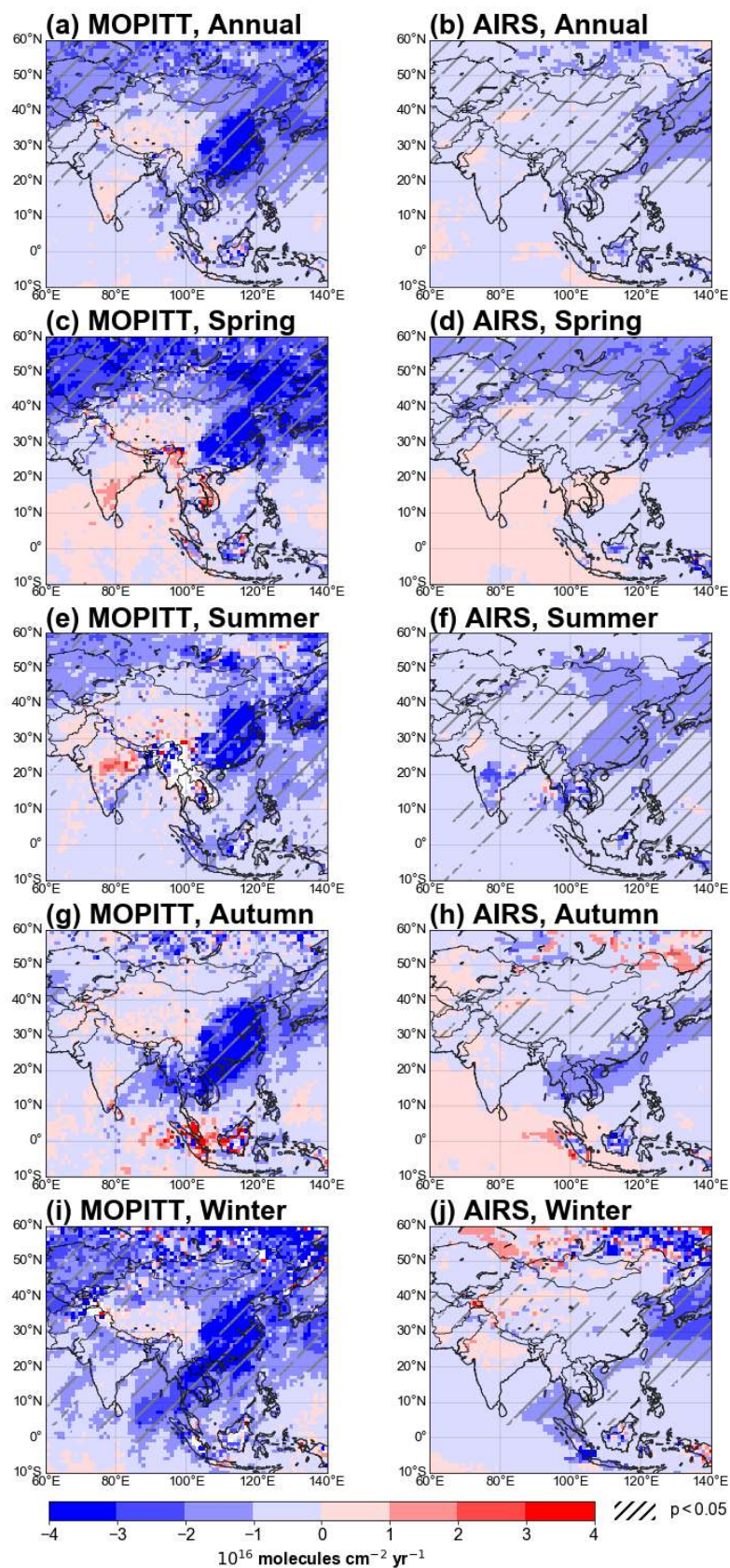
Figure 9. Horizontal distributions of the trends in CO total column during 2003–2017 from MOPITT (left column: (**a**) annual, (**c**) spring, (**e**) summer, (**g**) autumn, and (**i**) winter) and AIRS (right column: (**b**) annual, (**d**) spring, (**f**) summer, (**h**) autumn and (**j**) winter). The shadow indicates that the trends are statistically significant ($p < 0.05$).
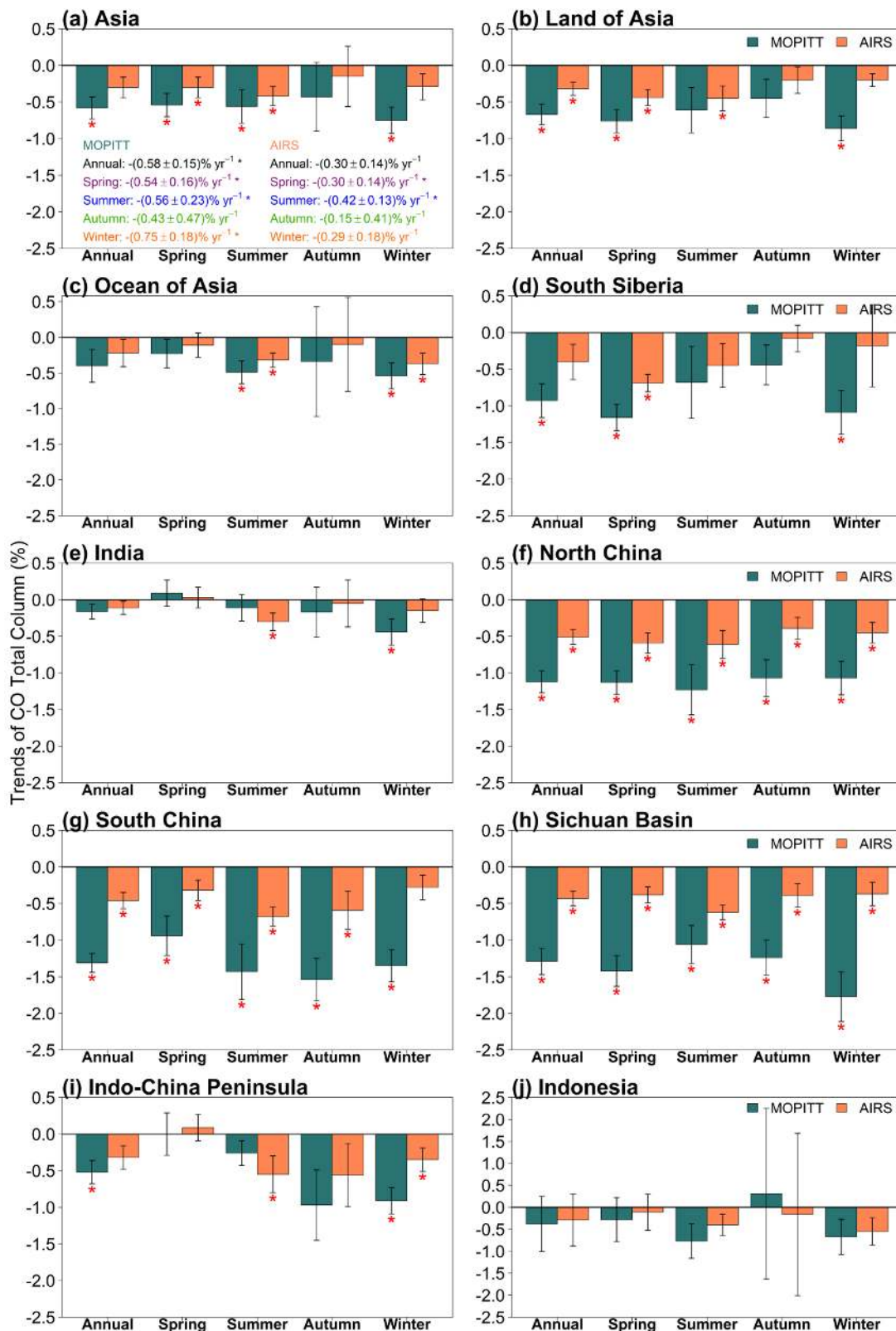
Figure 10. Trends in CO total columns (in %) from MOPITT and AIRS data averaged over Asia and its subregions during 2003–2017: (**a**) Asia, (**b**) the land of Asia, (**c**) the ocean of Asia, (**d**) South Siberia, (**e**) India, (**f**) North China, (**g**) South China, (**h**) the Sichuan Basin, (**i**) Indo-China Peninsula and (**j**) Indonesia. The red star indicates that the trend is statistically significant at 95% level (p < 0.05). The bar indicates the 95% confident interval.

Table 1. The trend in MOPITT CO total column (in 10^{17} molecules cm^{-2} per year) in the annual mean and by season over Asia and its subregions during 2003–2017 [1].

| Regions	Annual	Spring	Summer	Autumn	Winter
World	**−0.09 ± 0.02**	**−0.08 ± 0.04**	**−0.08 ± 0.02**	−0.08 ± 0.04	−0.07 ± 0.03
Asia	**−0.11 ± 0.03**	**−0.11 ± 0.03**	**−0.10 ± 0.04**	−0.08 ± 0.09	**−0.15 ± 0.04**
Asia (land)	**−0.13 ± 0.03**	**−0.17 ± 0.03**	**−0.12 ± 0.06**	−0.08 ± 0.05	**−0.17 ± 0.03**
Asia (ocean)	−0.07 ± 0.04	−0.04 ± 0.04	**−0.08 ± 0.03**	−0.06 ± 0.14	**−0.11 ± 0.04**
South Siberia	**−0.19 ± 0.05**	**−0.27 ± 0.04**	−0.14 ± 0.10	−0.08 ± 0.05	**−0.22 ± 0.06**
India	−0.03 ± 0.02	0.02 ± 0.04	−0.02 ± 0.03	−0.03 ± 0.07	**−0.10 ± 0.04**
North China	**−0.32 ± 0.04**	**−0.35 ± 0.05**	**−0.34 ± 0.10**	**−0.27 ± 0.06**	**−0.30 ± 0.06**
South China	**−0.36 ± 0.04**	**−0.29 ± 0.08**	**−0.32 ± 0.09**	**−0.40 ± 0.08**	**−0.39 ± 0.06**
Sichuan Basin	**−0.30 ± 0.04**	**−0.36 ± 0.05**	**−0.22 ± 0.05**	**−0.27 ± 0.05**	**−0.46 ± 0.09**
Indo-China Peninsula	**−0.13 ± 0.04**	−0.00 ± 0.08	−0.04 ± 0.03	−0.22 ± 0.11	**−0.23 ± 0.05**
Indonesia	−0.07 ± 0.12	−0.05 ± 0.09	−0.13 ± 0.07	0.06 ± 0.42	−0.14 ± 0.08

[1] Numbers in bold indicate that the trends are statistically significant at the 95% level ($p < 0.05$).

Figure 9 shows that the area with significant decreasing trend in CO total column from MOPITT is larger in spring and winter than in summer and autumn, and the decreasing trend in AIRS data is larger in spring and summer than in autumn and winter. The relative trends in MOPITT data averaged over Asia are found to be significant in all seasons except autumn (Figure 10a and Table 1). In North China, South China, and the Sichuan Basin, CO total column from both datasets decreases significantly in all seasons. In these subregions, CO total column observed by MOPITT declined at a rate of over 1% per year, while AIRS data declined at a rate of about 0.5% per year in all seasons (Figure 10f–h). Note that in India, CO total column from MOPITT decreases significantly only in winter (Figure 10e). In South Siberia, the decreasing trend is strongest in spring, as high as 1.16% and 0.69% per year, respectively, from MOPITT and AIRS observations (Figure 10d). In the Indo-China Peninsula, the decreasing trend is significant in winter (Figure 10i). In Indonesia, no significant trends are observed in all seasons (Figure 10j). Compared with the trends in CO total column over North China, South China, and the Sichuan Basin where anthropogenic emissions are high, the trends in CO total column over the fire-prone regions, i.e., South Siberia, the Indo-China Peninsula and Indonesia, appear weak or insignificant during the fire seasons (Figures 2, 9 and 10).

3.2. Correlations between Biomass Burning and the Interannual Variations and Trends in Atmospheric Carbon Monoxide over Asia

3.2.1. Sensitivity of the Interannual Variation in Carbon Monoxide over Asia to Biomass Burning

Biomass burning in Asia has strong interannual variation (Figure 11), which can significantly influence the year-to-year variation in CO total column in Asia. Tables 2 and 3 and Figure 12 show the correlation coefficients between CO total column and MODIS fire counts and between CO total column and GFED4 fire CO emissions over Asia. The annual mean of CO total column correlates significantly with the annual total fire counts, with r being 0.74 for MOPITT and 0.75 for AIRS, respectively (Figure 12a). Seasonally, the correlations averaged over Asia are significant in spring, summer, and autumn, and insignificant in winter (Figure 12c,e,g,i). The correlations between CO total column and fire counts over Asia appear stronger than those with fire CO emission data in all seasons (Figure 12c–j).
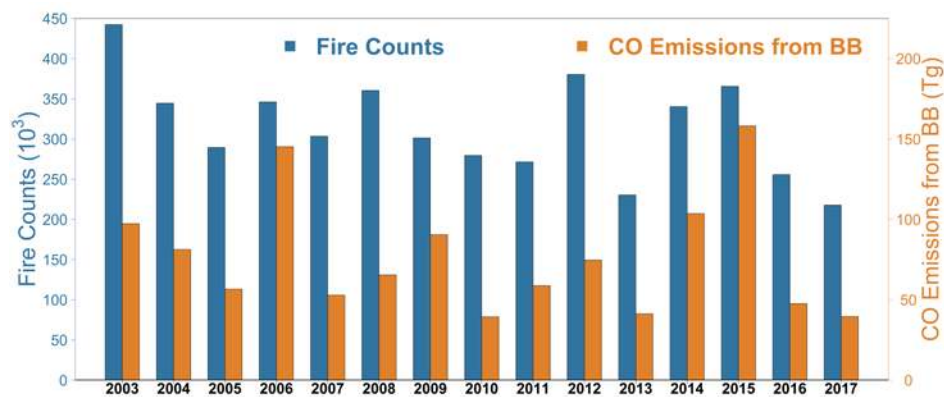
Figure 11. Interannual variations in the annual fire counts and annual CO emissions from biomass burning (BB) over Asia during 2003–2017.

Table 2. Correlation coefficients (r) between MOPITT CO total column and MODIS fire counts over different land covers in Asia and its subregions during 2003–2017 [1].

Regions	Land Cover	Annual	Spring	Summer	Autumn	Winter
Asia (land)	Forest	**0.79**	**0.71**	**0.77**	**0.54**	0.38
	Grassland	**0.72**	0.50	0.08	**0.70**	**−0.57**
	Shrubland	**0.55**	0.23	0.17	**0.82**	0.28
	Cropland	0.19	0.12	0.46	**0.74**	0.28
South Siberia	All	**0.77**	**0.72**	**0.73**	0.42	−0.01
India	All	−0.32	0.42	**0.56**	−0.37	−0.07
North China	All	−0.37	**−0.80**	0.04	−0.45	−0.49
South China	All	0.31	−0.04	−0.39	**0.61**	0.18
Sichuan Basin	All	−0.39	−0.09	**−0.60**	0.34	0.09
Indo-China Peninsula (land)	All	**0.60**	0.49	−0.23	**0.76**	**0.75**
Indonesia	All	**0.84**	**0.84**	**0.78**	**0.95**	**0.81**

[1] Numbers in bold indicate that the correlations are statistically significant at the 95% level (p < 0.05).

Table 3. Correlation coefficients (r) between MOPITT CO total column and GFED4 CO emissions from biomass burning over different land covers in Asia and its subregions during 2003–2017 [1].

Regions	Land Cover	Annual	Spring	Summer	Autumn	Winter
Asia (land)	Forest	**0.53**	**0.67**	**0.60**	**0.54**	0.41
	Grassland	**0.59**	0.36	−0.12	0.39	−0.26
	Shrubland	0.27	0.09	0.49	0.30	0.25
	Cropland	−0.04	−0.17	−0.01	0.51	0.12
South Siberia	All	**0.72**	**0.67**	**0.65**	−0.05	0.25
India	All	0.05	0.45	**0.52**	0.21	0.14
North China	All	**−0.53**	**−0.74**	−0.24	−0.43	**−0.58**
South China	All	−0.04	−0.19	**−0.57**	0.47	0.28
Sichuan Basin	All	**−0.86**	**−0.62**	**−0.83**	**−0.48**	−0.43
Indo-China Peninsula (land)	All	**0.62**	**0.55**	−0.22	0.45	**0.81**
Indonesia	All	**0.86**	**0.79**	**0.73**	**0.90**	**0.76**

[1] Numbers in bold indicate that the correlations are statistically significant at the 95% level (p < 0.05).
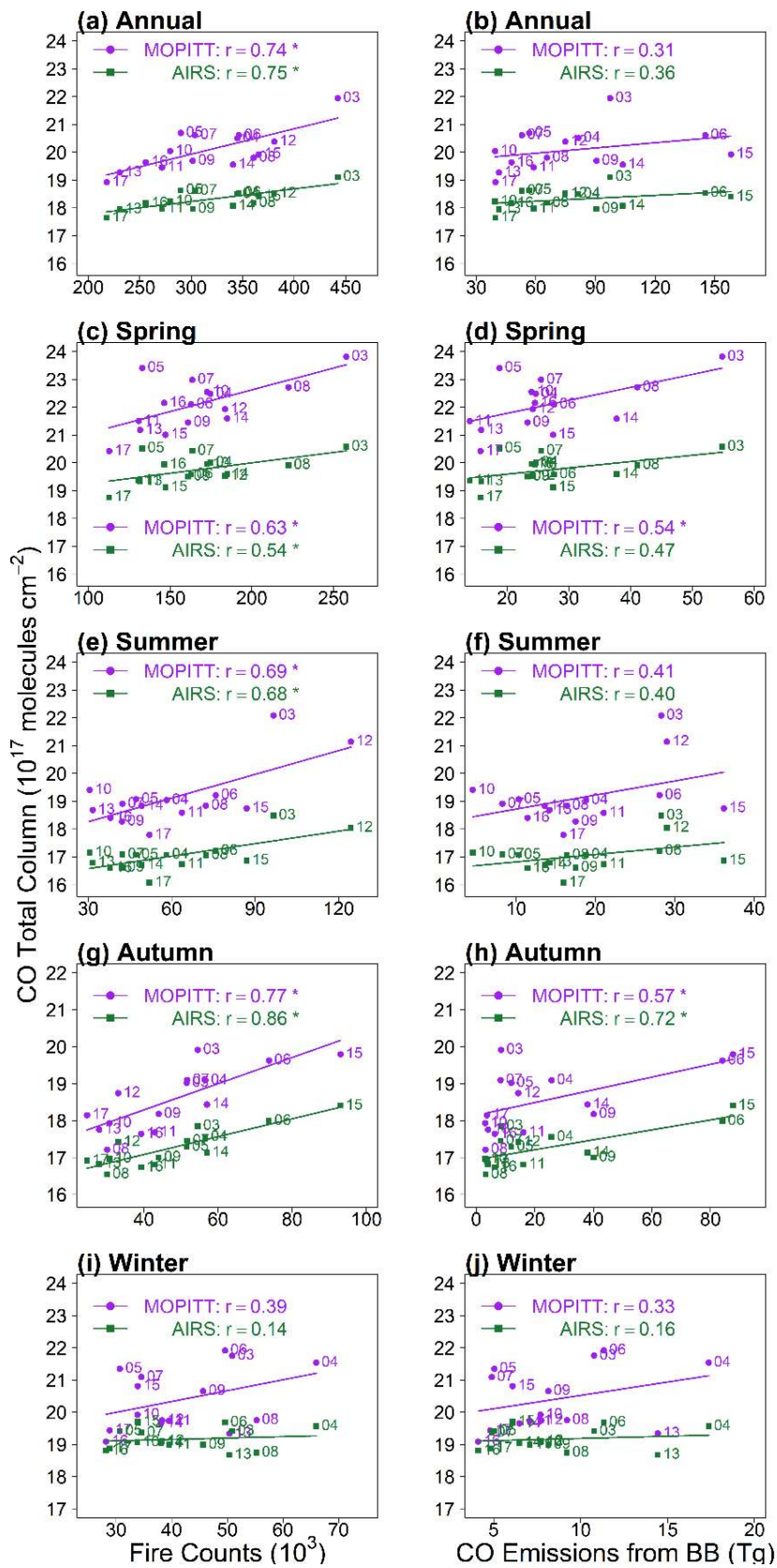
Figure 12. Correlation between CO total column and the MODIS fire counts (left column: (**a**) annual, (**c**) spring, (**e**) summer, (**g**) autumn and (**i**) winter) and between CO total column and the GFED4 CO emissions from biomass burning (right column: (**b**) annual, (**d**) spring, (**f**) summer, (**h**) autumn, and (**j**) winter) averaged over the land of Asia during 2003–2017. The star indicates that the trend is statistically significant at 95% level (p < 0.05). The number beside each dot denotes the last two digits of the year.

The correlation between the CO total column and biomass burning in different subregions are variant (Table 2). According to MOPITT data, the correlation is significant (p < 0.05) in three subregions: Indo-China (r = 0.60), South Siberia (r = 0.77), and Indonesia (r = 0.84). Seasonally, the correlation over Indonesia is significant in all seasons (r ranging between 0.78 and 0.95) and most significant in autumn, while over South Siberia, it is insignificant in autumn and winter (Table 2) when fires rarely occur (Figure 2). The correlations over the land of Indo-China Peninsula appear to be significant only in autumn and winter. Interestingly, only in autumn, the correlation is significant over the grassland (r = 0.70), shrubland (r = 0.82), and cropland (r = 0.74). Over forests, the correlation is significant in all seasons except in winter. Generally, the results from AIRS are similar to these from MOPITT (Table S3).

According to the CO fire emission data from GFED4, the correlation between CO total column and CO fire emissions is generally similar to but weaker than that between CO and MODIS fire counts in different subregions, land cover types, and seasons (Tables 2 and 3, Tables S3 and S4).

We explore the relationship between the extreme events of biomass burning and CO total column over Asia during 2003–2017 on regional mean. The annual total fire counts in Asia averaged over 2003–2017 is approximately 0.32 million (Figure 11). From 2003 to 2017, the annual total fire counts over Asia are highest in 2003, 2012, and 2015, with the values of 0.44, 0.38, and 0.37 million, respectively. In 2006, both MODIS fire counts and GFED4 CO emissions are high. The impact of biomass burning on CO can be illustrated in Figure 13, which shows the monthly anomalies of CO total column, fire counts, and fire CO emissions by latitude during 2003–2017. The extreme CO anomalies correspond to the strong fire events over some areas in Asia. The strong fire events occurs when CO anomalies are above 6×10^{17} molecules cm^{-2} in the satellite CO data in Figure 13, in which four extreme fire events are marked. The signature of the extreme fire events is well captured by MOPITT CO, MODIS fire counts, and GFED4 CO emissions from fires (see AIRS CO in Figure S1). When extreme fire events occur, positive anomalies of CO total column are observed over wide areas in Asia. Forest fires in eastern Russia in 2003, forest fires in Indonesia in 2006, wildfires in Siberia in 2012, and forest fires in Indonesia in 2015 can enhance the CO total column by 3×10^{17}, 3.4×10^{17}, 1.7×10^{17}, and 3.5×10^{17} molecules cm^{-2} over the fire-prone areas according to MOPITT observations (Figure 13a). The four extreme fire events largely contribute to the peaks of regional mean CO total column over Asia in 2003, 2006, 2012, and 2015 (Figure 7). Overall, biomass burning can largely explain the interannual variation in CO total column over Asia on regional mean.

3.2.2. Comparison of the Trend in Atmospheric Carbon Monoxide with the Trend in Biomass Burning in Asia

The decreasing trend in CO over Asia is probably associated with multiple factors, including anthropogenic and biomass emissions, atmospheric chemistry and dynamics. Few studies have focused on the impact of biomass burning on the CO trend over Asia [24]. Uncertainties in emission inventories also enhance the challenges of quantifying this impact [20,55]. In this section, we compare the trend in CO total column over Asia and the trend in biomass burning, to explore a linkage between the two. Since CO emitted from biomass burning can be transported across continents [56–58], the trends in biomass burning both inside and outside Asia are examined.

As shown in Section 3.1.3, CO total column over Asia from MOPITT decreases significantly in all seasons except autumn (Figure 10). Figure 14 compares the trend in CO total column in Asia with the trends in four datasets, i.e., MODIS fire counts inside and outside Asia, and GFED4 CO fire emissions inside and outside Asia. In spring, the fire counts inside and outside Asia decrease significantly; CO fire emissions inside and outside Asia decrease at a significant level of 86% and 89%, respectively. The trends in the four datasets indicate that global biomass burning may be a potential driver of the decreasing trend in CO total column over Asia in spring. However, in other seasons, among the four datasets, only fire counts outside Asia decrease significantly in autumn and winter. In summer, global biomass burning may not be a driver for the decreasing trend in CO total column over Asia. In winter, the biomass burning outside Asia has a low probability to be a cause of the decreasing trend in CO total column over Asia.
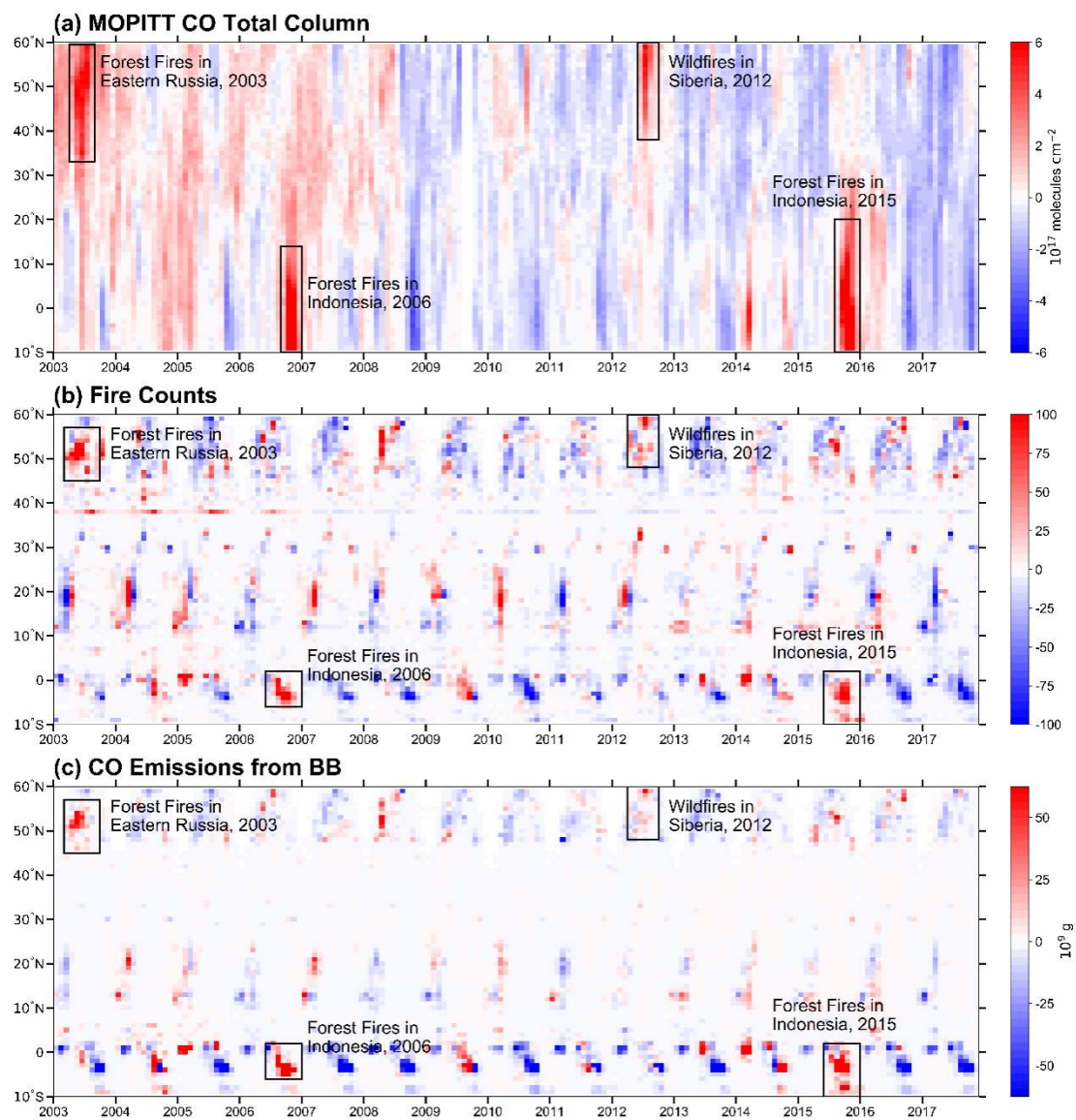
Figure 13. Monthly variations in the anomalies of (**a**) MOPITT CO total column, (**b**) fire counts, and (**c**) CO emissions from biomass burning (BB) averaged over 60–140°E during 2003–2017. Rectangles mark the extreme fire events.
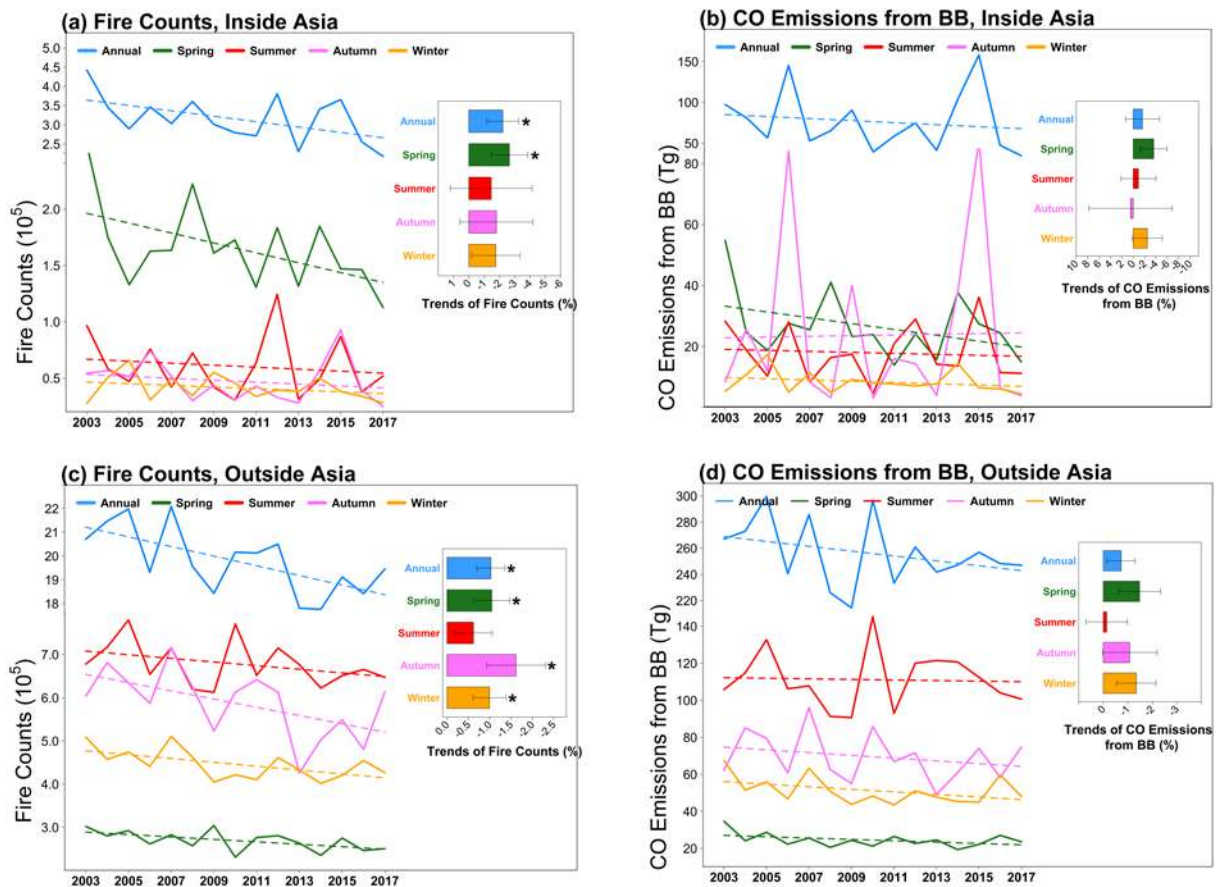
Figure 14. Interannual variations and trends in MODIS fire counts and GFED4 fire emissions in the annual mean and by season: (**a**) fire counts inside Asia, (**b**) fire CO emissions inside Asia, (**c**), fire counts outside Asia, (**d**) fire CO emissions outside Asia. The black star indicates that the trend is statistically significant (p < 0.05).

4. Discussion

4.1. Temporal–Spatial Variations and Trends in Atmospheric Carbon Monoxide over Asia

Previous studies showed that Asia is one of the most polluted regions, and CO hotspots were observed over East Asia and East India [59,60]. Over 2003–2017, the values of CO total column from MOPITT and AIRS are high in most areas of East Asia and Indo-China Peninsula (Figure 4). Intensive traffic and industrial activities, urbanization, and large population density in these areas lead to high levels of anthropogenic CO emissions [17,24,29]. On regional average, atmospheric CO column in Asia observed by MOPITT in spring and winter is higher than in summer and autumn, in agreement with the seasonality of CO columns from AIRS (Figure 6).

The values of CO total column from MOPITT and AIRS show strong interannual variation in Asia (Figures 7 and 8), and CO peaked in the years of 2003, 2006, 2009, 2012 and 2015. Some of the peaks are probably due to large fire events under dry conditions (i.e., the years of El Niño) [39,61], especially in spring and summer over South Siberia [3,37], and in autumn and winter in Indonesia [32,40]. According to MOPITT data, the CV of the annual mean CO total column over Asia is 5.8%, which is weaker than that over the world (8.3%). The CV is higher in the regions with more biomass burning [27] (Figure 2a and 8a). The CV is lowest in India, likely due to small interannual variations in emissions of CO from anthropogenic activities and biomass burning.

Worden et al. [19] found that all nadir-viewing thermal infrared (TIR) satellites measurements of CO total column are with a significantly decreasing trend ~1% yr^{-1} at the 1σ level over the Northern

Hemisphere from 2000 to 2011. Our results show that the annual mean CO total column in Asia declined at an average rate of 0.58% yr^{-1} from 2003 to 2017 in MOPITT data (p < 0.05). CO total column in Asia has decreased continuously since 2011 after Worden's analysis. Figure 9 shows that the decreasing trends in CO total column from MOPITT is strongest in East China, with a rate of $-0.2 \sim -0.4 \times 10^{17}$ molecules cm^{-2} per year. Previous studies showed that the decreasing trends are mainly caused by rapid technological changes with improved combustion efficiency and emission control measures in China since 2010 [32,55,62]. Note that in India, the annual and seasonal trends in MOPITT CO columns are smallest among all the subregions and all the decreasing trends are insignificant except in winter; there even is an insignificant increasing trend in spring. Contrary to China, the anthropogenic emissions in India have increased during the study period [24,55]. The increase of anthropogenic emissions over India may partially offset the overall decreasing trend in Asia and lead to smaller decreasing trends in India than in the rest of Asia. In addition, Yuan et al. [63] reported that CO has increased in the Asian Tropopause Aerosol Layer, a planetary-scale aerosol layer situated 13–18 km above sea level partially covering the northern part of India. This amount of CO and its variation are detected by satellite instruments. This may also be a reason why the trend in CO total column over India is among the smallest in Asia.

In general, the trends in CO total column over the fire-prone regions are found to be weak during their corresponding fire seasons. This leads to the next section where we discuss the impacts of biomass burning on the interannual variation and trend in atmospheric CO over Asia in further detail.

4.2. Impacts of Biomass Burning on the Interannual Variation and Trend in Atmospheric Carbon Monoxide over Asia

The interannual variation in CO total column appears to be sensitive to biomass burning in Asia and its subregions. In Asia, MODIS fire counts and GFED4 CO emissions show strong interannual variations, and high values often coincide with EI Niño years [64]. As seen in Figures 7 and 11, the years with peak CO total column often coincide with the years of peak fire counts or CO emissions from fires or both. On the annual average, the correlation coefficients between CO total column and fire counts is 0.74 from MOPITT data and 0.75 from AIRS data (p < 0.05). However, although the GFED4 data also suggest a positive correlation between CO total column and CO emissions from biomass burning in Asia, the correlation is not significant (r = 0.31–0.36, *p* > 0.05) (Figure 12a,b). Seasonally (Figure 12c–j), the fire count data suggest strong correlations between fires and CO total column in all seasons except in winter using both MOPITT and AIRS CO data, while the CO emission data only show strong correlations in autumn in both CO datasets and in summer in MOPITT CO data. The fire counts in spring comprise 52.5% of the total annual fire counts and springtime CO emissions from fires are the highest among all seasons (34.7%). In autumn, the fire counts comprise 15% of the total annual fire counts and the CO emissions form fires are the second highest (30.9%).

Overall, biomass burning occurs mostly in spring and autumn over Asia in 2003–2017, CO total column is sensitive to variation in biomass burning. High CO levels were observed during the intensive biomass burning events (Figure 13) [37,40,41]. For example, wildfires in Siberia in 2003 and forest fires in Indonesia in 2015 can enhance the abundances of CO by 3×10^{17} and 3.5×10^{17} molecules cm^{-2} over the fire-prone areas according to MOPITT measurements.

Tables 2 and 3 show how the interannual variation in CO total column coincide with that in fire occurrences in different land cover types and over different subregions of Asia. Because forest fires account for ~50% of the total fire counts or CO emissions from fires (Figure 3c–d), plus the fact that the emission factors of forest fires are one of the highest among all land cover types, forest fires have a significant impact on the interannual variations in CO columns from both MOPITT and AIRS data over the land of Asia (r = 0.54–0.79), in all seasons except in winter. Interestingly, over cropland, grassland, and shrubland, fire counts only significantly correlate with CO columns in autumn over the land of Asia (r = 0.70–0.82). By subregion, there is a positive and significant correlation between CO total column and biomass burning in the fire-prone seasons and areas, for example, in spring, summer over South Siberia (r = 0.65–0.73), and in all seasons over Indonesia (r = 0.73–0.95). Positive correlations are

usually found in fire-prone regions [3,24,47], e.g., in winter over the land of Indo-China Peninsula. Yin et al. [25] also reported a significant correlation (r = 0.82) between monthly MOPITT CO total column and fire counts in Southeast Asia during the fire season (December–May). However, in the regions with strong anthropogenic emissions and few fire activities [15,18,32,65], negative correlations between CO columns and fire counts can appear, e.g., India, North China, and the Sichuan Basin in the annual mean, North China in spring, and the Sichuan Basin in summer.

Interpreting the decreasing trends in atmospheric CO in Asia requires accurate evolution of CO concentrations between multiple CO emissions sources (i.e., anthropogenic emissions, biomass burning emissions, biogenic and oceanic emissions, and chemical production) and the CO sinks (i.e., the CO chemical sink and dry deposition) [2,24]. Zheng et al. [24] stated that CO from chemical production, as well as from oceanic and biogenic sources changes a little on a global scale. In contrast, atmospheric transport play a confounding role in modulating the CO trends in a receptor region [5,34,56]. Zheng et al. [24] identified a declining trend in the global CO budget in 2000–2017, driven by reduced anthropogenic emissions in the US, Europe, and China, as well as by reduced biomass burning emissions globally. In this study, the declining trend in the annual total fire counts inside Asia is revealed (Figure 14a), which is mainly attributable to declining fire counts in spring. However, the GFED4 fire emission data show no significant trend inside Asia in all seasons (Figure 14b). Outside Asia, the downward trend in fire counts is statistically significant in all seasons except in summer (Figure 14c), while no significant trends in the GFED4 CO emissions are shown (Figure 14d). As the GFED4 data show a different sensitivity of CO trend to biomass burning, future work using numerical models and observation evidence is needed to further address the issue. The deceasing trends in fire accounts inside and outside Asia are probably attributable to the following reasons. First, land use change (i.e., the expansion of crop and pasture lands leads to more burned areas but fewer emissions globally. Second, fires are suppressed more due to increased human efforts [52]. Third, the globe becomes wetter in the second half of the twentieth century in most regions of Asia [66] (i.e., western China, Central Asia, India subcontinent, and Indonesia).

There are multiple factors affecting the spatial variations and trends in CO total column among different subregions in Asia. For example, in China, these factors include uneven distributions of economic development, population, meteorology [56], farming techniques (i.e., the control of chemical fertilizers, the strict straw open burning ban policy) [67,68], and the region-specific forest management strategies (i.e., forest fire prevention) [69], which would result in a CO trend downward or upward. In South Asia and Indonesia, land cover use change (i.e., urbanization), and farming techniques (i.e., the expansion of crop and pasture lands) [66] likely lead to strong CO emissions. The length of the fire seasons in the southern Siberia (virgin boreal forest) has been projected to increase by at least one month due to the lack of precipitation [51,70], drier climate; higher fire danger would likely lead to huge CO emissions from fires. Pan et al. [71] found that fires are always more intensive in southern Kalimantan than in southern Sumatra in all EI Niño events in 1979–2016. More intense and prolonged Indonesian drought and fires occur in the Eastern Pacific type, during which the emitted carbon amounts almost double those in the Central Pacific type.

4.3. Comparison of Atmospheric Carbon Monoxide over Asia Observed by MOPITT and AIRS

In this study, we used two sets of satellite CO data to demonstrate the spatial–temporal variations in atmospheric CO over Asia to enhance confidence for our analysis. Although MOPITT and AIRS CO columns have a significant correlation over Asia up to 0.98 in all seasons (Figure 5), some discrepancies between the MOPITT and the AIRS CO data are observed. First, both long-term mean and standard deviation of CO total column from MOPITT are higher than those from AIRS. Second, the mean CV from MOPITT (5.8%) is higher than that from AIRS (4.1%) over Asia, suggesting a larger interannual variation. Third, the decreasing trend in the annual mean of CO total column from MOPITT (−0.58% per year) is stronger than that from AIRS (−0.30% per year) over Asia. Fourthly, discrepancies between MOPITT and AIRS CO data are apparent in different seasons, among different subregions, and over

different land covers, in terms of CO abundances, temporal-spatial variations, and sensitivity of CO to biomass burning (Tables S2–S4 and Figure S1).

These differences are likely due to multiple factors. First, MOPITT and AIRS uses different instruments; one uses a gas correlation radiometer and the other uses grating spectrometer. Second, at the nadir, the ground footprint of MOPITT measurement is 22 km × 22 km, and the scan angle of 26.1° across the satellite flight track (640 km) allows a global coverage in 2.5 days [19,59,72], while AIRS has 13.5 km × 13.5 km footprint, and its swath (1650 km) provides near global coverage twice daily [19,73]. Therefore, MOPITT can capture high CO hotspots and result in high spatial variation [8], while AIRS data cover significantly large areas daily.

The MOPITT CO retrieval algorithm is a maximum a posteriori method that incorporates a priori information of the physical and statistical variability of the trace gas distribution in the atmosphere to choose the best solution [72,74]. Compared to CO retrievals from MOPITT, the current AIRS physical retrieval algorithm seeks to minimize the weighted difference between the clear column radiance observations [75] and the radiances computed using a forward model [8,76] by varying the geophysical state.

The AIRS CO retrievals use reconstructed cloudy grids while MOPITT removes cloudy grids [72,73,77]. Due to the lack of sensitivity in the lower troposphere for down-looking spectrometers such as AIRS [8], when the total column CO amount is high over the land in the Northern Hemisphere, AIRS CO columns are lower than MOPITT CO (Figure 5b). Over the oceans, AIRS CO columns are slightly larger than MOPITT CO (Figure 5c).

5. Conclusions

Using MOPITT and AIRS satellite data, which have high accuracy and long-term coverage, we investigated the seasonal and interannual variations, and the long-term trends in atmospheric CO in Asia over 2003–2017. Combing with the datasets of MODIS fire counts and GFED4 fire emissions, we explored the influences of biomass burning on the long-term variation and trends in atmospheric CO in Asia over different regions and different land covers.

CO total column over Asia from MOPITT is slightly higher than that from AIRS, and the two datasets show similar spatial and seasonal patterns. On annual average, CO columns over Asia from MOPITT and AIRS are $(19.3 \pm 4.3) \times 10^{17}$ molecules cm^{-2} and $(18.5 \pm 2.8) \times 10^{17}$ molecules cm^{-2}, respectively. The correlation coefficient between the two datasets ranges from 0.86 to 0.98 over Asia, being lowest over the Tibetan Plateau and India. CO total column over most areas in Asia exhibits a strong seasonality, being higher in spring and winter than in summer and autumn. The interannual variation in CO total column is large over Asia, with a regional mean CV of 5.8% in MOPITT data, although the CV is lower than the global mean.

The seasonal and interannual variations in CO total column over Asia is greatly impacted by biomass burning, especially over South Siberia, Indo-China Peninsula, and Indonesia. CO total column in Asia correlates more closely with MODIS fire counts than with GFED4 fire emissions. On annual mean, the correlation coefficient between MODIS fire counts and MOPITT CO total column over Asia reaches 0.76. MODIS fire counts may explain 60%, 36%, and 71% of the interannual variation in the annual mean CO total column over South Siberia, Indo-China Peninsula, and Indonesia, respectively. Meanwhile, MODIS fire counts may explain 62%, 52%, and 31% of the interannual variation in the annual mean CO total column, respectively, over forest, grassland, and shrubland in Asia. During 2003–2017, the peaks of CO total column over Asia are closely correlate to the extreme fire events, for instance, the severe fires over Siberia in 2003 and 2012 and over Indonesia in 2006 and 2015. The extreme fire events can remarkably increase the CO total column over Asia, which are observed by the MOPITT and AIRS.

From 2003 to 2017, according to MOPITT data, CO total column in Asia decreased significantly at a rate of $-(0.58 \pm 0.15)$% (or $-(0.11 \pm 0.03) \times 10^{17}$ molecules cm^{-2}) per year. The decreasing trend is significant over land but insignificant over oceans. Over land, the decreasing trend is most obvious over

North China, South China, and the Sichuan Basin, with a regional mean over 1% per year. However, over India and Indonesia, no significant trends in the annual mean CO total column are observed. Seasonally, the decreasing trend over Asia is most significant in winter, following by summer and spring, while the decreasing trend in autumn is not significant. The declines of MODIS fire counts inside and outside Asia over 2003–2017 suggest that biomass burning may be one of the reasons for the decreasing trend in CO total column in Asia, especially in spring, although the decreasing trends in the GFED4 fire emission data are insignificant.

Based on satellite observations and statistical analysis, this study demonstrates the spatial variations and long-term trends in atmospheric CO over Asia and their sensitivities to biomass burning. The results help further understand the role of CO in atmospheric chemistry, air pollution, and carbon cycle. In the future, numerical simulations are needed to further quantify the contributions of various factors to the trends in atmospheric CO over Asia, including the influences of emissions from both anthropogenic activities and biomass burning.

Supplementary Materials: The following are available online at http://www.mdpi.com/2072-4292/12/5/830/s1, Table S1: Land cover classification on the basis of the ESA CCI Land Cover, Table S1: The trends of AIRS CO total column in Asia, its sub-regions, and the world, Table S3: Correlation coefficients (r) between AIRS CO total column and the number of MODIS fire counts over different land cover and sub-regions in Asia during 2009–2017, Table S4: Correlation coefficients (r) between AIRS CO total column and the GFED4 CO emissions from biomass burning over different land covers and sub-regions in Asia during 2003–2017, Figure S1: Monthly variations in the anomalies of AIRS CO total column.

Author Contributions: X.Z. and J.L. designed the research. X.Z. performed the research and analyzed the data. H.H., X.Z. and J.L. wrote the paper. Y.Z., Z.J., H.W., L.M., Y.C.L., and Y.L. contributed to the analysis and presentation. All authors have read and agreed to the published version of the manuscript.

Conflicts of Interest: The authors declare no conflicts of interest.

References

1. Holloway, T.; Levy Ii, H.; Kasibhatla, P. Global distribution of carbon monoxide. *J. Geophys. Res. Atmos.* **2000**, *105*, 12123–12147. [CrossRef]

2. Jacob, D.J. *Introduction to Atmospheric Chemistry*; Princeton University Press: Princeton, NJ, USA, 2000.

3. Yurganov, L.N.; McMillan, W.W.; Dzhola, A.V.; Grechko, E.I.; Jones, N.B.; Van der Werf, G.R. Global AIRS and MOPITT CO measurements: Validation, comparison, and links to biomass burning variations and carbon cycle. *J. Geophys. Res. Atmos.* **2008**, *113*, D09301. [CrossRef]

4. Logan, J.A.; Prather, M.J.; Wofsy, S.C.; McElroy, M.B. Tropospheric chemistry: A global perspective. *J. Geophys. Res. Oceans* **1981**, *86*, 7210–7254. [CrossRef]

5. Ding, K.; Liu, J.; Ding, A.; Liu, Q.; Zhao, T.L.; Shi, J.; Han, Y.; Wang, H.; Jiang, F. Uplifting of carbon monoxide from biomass burning and anthropogenic sources to the free troposphere in East Asia. *Atmos. Chem. Phys.* **2015**, *15*, 2843–2866. [CrossRef]

6. Drummond, J.R.; Mand, G.S. The Measurements of Pollution in the Troposphere (MOPITT) Instrument: Overall Performance and Calibration Requirements. *J. Atmos. Ocean. Technol.* **1996**, *13*, 314–320. [CrossRef]

7. Deeter, M.N.; Edwards, D.P.; Gille, J.C.; Drummond, J.R. Sensitivity of MOPITT observations to carbon monoxide in the lower troposphere. *J. Geophys. Res. Atmos.* **2007**, *112*, D24. [CrossRef]

8. Warner, J.; Comer, M.M.; Barnet, C.D.; McMillan, W.W.; Wolf, W.; Maddy, E.; Sachse, G. A comparison of satellite tropospheric carbon monoxide measurements from AIRS and MOPITT during INTEX-A. *J. Geophys. Res. Atmos.* **2007**, *112*, D12. [CrossRef]

9. Bremer, H.; Kar, J.; Drummond, J.R.; Nichitu, F.; Zou, J.; Liu, J.; Gille, J.C.; Deeter, M.N.; Francis, G.; Ziskin, D.; et al. Spatial and temporal variation of MOPITT CO in Africa and South America: A comparison with SHADOZ ozone and MODIS aerosol. *J. Geophys. Res. Atmos.* **2004**, *109*, 12301–12310. [CrossRef]

10. Clerbaux, C.; Boynard, A.; Clarisse, L.; George, M.; Hadji-Lazaro, J.; Herbin, H.; Hurtmans, D.; Pommier, M.; Razavi, A.; Turquety, S.; et al. Monitoring of atmospheric composition using the thermal infrared IASI/MetOp sounder. *Atmos. Chem. Phys.* **2009**, *9*, 6041–6054. [CrossRef]

11. Palve, S.N.; Nemade, P.D.; Ghude, S.D. MOPITT carbon monoxide its source distributions, interannual variability and transport pathways over India during 2005-2015. *Int. J. Remote Sens.* **2018**, *39*, 5952–5964. [CrossRef]

12. Zhang, L.; Jiang, H.; Lu, X.; Jin, J. Comparison analysis of global carbon monoxide concentration derived from SCIAMACHY, AIRS, and MOPITT. *Int. J. Remote Sens.* **2016**, *37*, 5155–5175. [CrossRef]

13. Kar, J.; Jones, D.B.A.; Drummond, J.R.; Attié, J.L.; Liu, J.; Zou, J.; Nichitiu, F.; Seymour, M.D.; Edwards, D.P.; Deeter, M.N.; et al. Measurement of low-altitude CO over the Indian subcontinent by MOPITT. *J. Geophys. Res. Atmos.* **2008**, *113*, D16. [CrossRef]

14. Gloudemans, A.M.S.; De Laat, A.T.J.; Schrijver, H.; Aben, I.; Meirink, J.F.; Van Der Werf, G.R. SCIAMACHY CO over land and oceans: 2003-2007 interannual variability. *Atmos. Chem. Phys.* **2009**, *9*, 3799–3813. [CrossRef]

15. Girach, I.A.; Nair, P.R. Carbon monoxide over Indian region as observed by MOPITT. *Atmos. Environ.* **2014**, *99*, 599–609. [CrossRef]

16. Ul-Haq, Z.; Rana, A.D.; Ali, M.; Mahmood, K.; Tariq, S.; Qayyum, Z. Carbon monoxide (CO) emissions and its tropospheric variability over Pakistan using satellite-sensed data. *Adv. Space Res.* **2015**, *56*, 583–595. [CrossRef]

17. Osman, M.K.; Tarasick, D.W.; Liu, J.; Moeini, O.; Thouret, V.; Fioletov, V.E.; Parrington, M.; Nédélec, P. Carbon monoxide climatology derived from the trajectory mapping of global MOZAIC-IAGOS data. *Atmos. Chem. Phys.* **2016**, *16*, 10263–10282. [CrossRef]

18. Bai, W.; Zhang, P.; Zhang, X.; Wang, W.; Qi, J.; Liu, H.; Zhang, W.; Bianba, C. Temporal and spatial distribution characteristics of carbon monoxide column amount over China based on satellite data. *J. Appl. Meteorol. Sci.* **2010**, *21*, 473–483.

19. Worden, H.M.; Deeter, M.N.; Frankenberg, C.; George, M.; Nichitiu, F.; Worden, J.; Aben, I.; Bowman, K.W.; Clerbaux, C.; Coheur, P.F.; et al. Decadal record of satellite carbon monoxide observations. *Atmos. Chem. Phys.* **2013**, *13*, 837–850. [CrossRef]

20. Jiang, Z.; Jones, D.B.A.; Worden, H.M.; Henze, D.K. Sensitivity of top-down CO source estimates to the modeled vertical structure in atmospheric CO. *Atmos. Chem. Phys.* **2015**, *15*, 1521–1537. [CrossRef]

21. Duncan, B.N.; Logan, J.A.; Bey, I.; Megretskaia, I.A.; Yantosca, R.M.; Novelli, P.C.; Jones, N.B.; Rinsland, C.P. Global budget of CO, 1988–1997: Source estimates and validation with a global model. *J. Geophys. Res. Atmos.* **2007**, *112*, D22. [CrossRef]

22. Wang, P.; Elansky, N.F.; Timofeev, Y.M.; Wang, G.; Golitsyn, G.S.; Makarova, M.V.; Rakitin, V.S.; Shtabkin, Y.; Skorokhod, A.I.; Grechko, E.I.; et al. Long-term trends of carbon monoxide total columnar amount in urban areas and background regions: Ground- and satellite-based spectroscopic measurements. *Adv. Atmos. Sci.* **2018**, *35*, 785–795. [CrossRef]

23. Ul-Haq, Z.; Tariq, S.; Ali, M. Anthropogenic emissions and space-borne observations of carbon monoxide over South Asia. *Adv. Space Res.* **2016**, *58*, 1610–1626. [CrossRef]

24. Zheng, B.; Chevallier, F.; Yin, Y.; Ciais, P.; Fortems-Cheiney, A.; Deeter, M.N.; Parker, R.J.; Wang, Y.; Worden, H.M.; Zhao, Y. Global atmospheric carbon monoxide budget 2000-2017 inferred from multi-species atmospheric inversions. *Earth Sys. Sci. Data* **2019**, *11*, 1411–1436. [CrossRef]

25. Yin, S.; Wang, X.; Zhang, X.; Guo, M.; Miura, M.; Xiao, Y. Influence of biomass burning on local air pollution in mainland Southeast Asia from 2001 to 2016. *Environ. Pollut.* **2019**, *254*, 112949. [CrossRef] [PubMed]

26. Granier, C.; Bessagnet, B.; Bond, T.; D'Angiola, A.; van der Gon, H.D.; Frost, G.J.; Heil, A.; Kaiser, J.W.; Kinne, S.; Klimont, Z.; et al. Evolution of anthropogenic and biomass burning emissions of air pollutants at global and regional scales during the 1980–2010 period. *Clim. Chang.* **2011**, *109*, 163–190. [CrossRef]

27. Van Der Werf, G.R.; Randerson, J.T.; Giglio, L.; Van Leeuwen, T.T.; Chen, Y.; Rogers, B.M.; Mu, M.; Van Marle, M.J.E.; Morton, D.C.; Collatz, G.J.; et al. Global fire emissions estimates during 1997–2016. *Earth Syst. Sci. Data* **2017**, *9*, 697–720. [CrossRef]

28. Sinha, P.; Hobbs, P.V.; Yokelson, R.J.; Blake, D.R.; Gao, S.; Kirchstetter, T.W. Distributions of trace gases and aerosols during the dry biomass burning season in southern Africa. *J. Geophys. Res. Atmos.* **2003**, *108*, ACH 4-1–ACH 4-23. [CrossRef]

29. Kganyago, M.; Shikwambana, L. Assessing spatio-temporal variability of wildfires and their impact on sub-Saharan ecosystems and air quality using multisource remotely sensed data and trend analysis. *Sustainability* **2019**, *11*, 6811. [CrossRef]

30. Zheng, B.; de Beurs, K.M.; Owsley, B.C.; Henebry, G.M. Scaling relationship between CO pollution and population size over major US metropolitan statistical areas. *Landsc. Urban Plan.* **2019**, *187*, 191–198. [CrossRef]

31. Liu, J.; Drummond, J.R.; Li, Q.; Gille, J.C.; Ziskin, D.C. Satellite mapping of CO emission from forest fires in Northwest America using MOPITT measurements. *Remote Sens. Environ.* **2005**, *95*, 502–516. [CrossRef]

32. Zheng, B.; Chevallier, F.; Ciais, P.; Yin, Y.; Deeter, M.N.; Worden, H.M.; Wang, Y.; Zhang, Q.; He, K. Rapid decline in carbon monoxide emissions and export from East Asia between years 2005 and 2016. *Environ. Res. Lett.* **2018**, *13*, 44007. [CrossRef]

33. Kang, H.Q.; Zhu, B.; van der A, R.J.; Zhu, C.M.; de Leeuw, G.; Hou, X.W.; Gao, J.H. Natural and anthropogenic contributions to long-term variations of SO2, NO2, CO, and AOD over East China. *Atmos. Res.* **2019**, *215*, 284–293. [CrossRef]

34. Li, Y.; Liu, J.; Han, H.; Zhao, T.; Zhang, X.; Zhuang, B.; Wang, T.; Chen, H.; Wu, Y.; Li, M. Collective impacts of biomass burning and synoptic weather on surface PM2.5 and CO in Northeast China. *Atmos. Environ.* **2019**, *213*, 64–80. [CrossRef]

35. Paton-Walsh, C.; Deutscher, N.M.; Griffith, D.W.T.; Forgan, B.W.; Wilson, S.R.; Jones, N.B.; Edwards, D.P. Trace gas emissions from savanna fires in northern Australia. *J. Geophys. Res. Atmos.* **2010**, *115*, D16314. [CrossRef]

36. Yurganov, L.N.; Blumenstock, T.; Grechko, E.I.; Hase, F.; Hyer, E.J.; Kasischke, E.S.; Koike, M.; Kondo, Y.; Kramer, I.; Leung, F.Y.; et al. A quantitative assessment of the 1998 carbon monoxide emission anomaly in the Northen Hemisphere based on total column and surface concentration measurements. *J. Geophys. Res. Atmos.* **2004**, *109*, 15301–15313. [CrossRef]

37. Yurganov, L.N.; Duchatelet, P.; Dzhola, A.V.; Edwards, D.P.; Hase, F.; Kramer, I.; Mahieu, E.; Mellqvist, J.; Notholt, J.; Novelli, P.C.; et al. Increased Northern Hemispheric carbon monoxide burden in the troposphere in 2002 and 2003 detected from the ground and from space. *Atmos. Chem. Phys.* **2005**, *5*, 563–573. [CrossRef]

38. Lalitaporn, P.; Kurata, G.; Matsuoka, Y.; Thongboonchoo, N.; Surapipith, V. Long-term analysis of NO2, CO, and AOD seasonal variability using satellite observations over Asia and intercomparison with emission inventories and model. *Air Qual. Atmos. Health* **2013**, *6*, 655–672. [CrossRef]

39. Streets, D.G.; Yarber, K.F.; Woo, J.H.; Carmichael, G.R. Biomass burning in Asia: Annual and seasonal estimates and atmospheric emissions. *Glob. Biogeochem. Cycles* **2003**, *17*, 10–11. [CrossRef]

40. Worden, J.; Jiang, Z.; Jones, D.B.A.; Alvarado, M.; Bowman, K.; Frankenberg, C.; Kort, E.A.; Kulawik, S.S.; Lee, M.; Liu, J.; et al. El Niño, the 2006 Indonesian peat fires, and the distribution of atmospheric methane. *Geophys. Res. Lett.* **2013**, *40*, 4938–4943. [CrossRef]

41. Nechita-Banda, N.; Krol, M.; Van Der Werf, G.R.; Kaiser, J.W.; Pandey, S.; Huijnen, V.; Clerbaux, C.; Coheur, P.; Deeter, M.N.; Röckmann, T. Monitoring emissions from the 2015 Indonesian fires using CO satellite data. *Philos. Trans. R. Soc. B Biol. Sci.* **2018**, *373*. [CrossRef]

42. Ziskin, D. *MOPITT Level 3 CO Gridded Monthly Means (Near and Thermal Infrared Radiances) HDF File-Version 7*; NASA Langley Research Center Atmospheric Science Data Center DAAC: Hampton, VA, USA, 2016. [CrossRef]

43. Warner, J.; Carminati, F.; Wei, Z.; Lahoz, W.; Attié, J.L. Tropospheric carbon monoxide variability from AIRS under clear and cloudy conditions. *Atmos. Chem. Phys.* **2013**, *13*, 12469–12479. [CrossRef]

44. McMillan, W.W.; Evans, K.D.; Barnet, C.D.; Maddy, E.S.; Sachse, G.W.; Diskin, G.S. Validating the AIRS version 5 CO retrieval with DACOM in situ measurements during INTEX-A and -B. *IEEE Trans. Geosci. Remote Sens.* **2011**, *49*, 2802–2813. [CrossRef]

45. Miyazaki, K.; Eskes, H.J.; Sudo, K. A tropospheric chemistry reanalysis for the years 2005-2012 based on an assimilation of OMI, MLS, TES, and MOPITT satellite data. *Atmos. Chem. Phys.* **2015**, *15*, 8315–8348. [CrossRef]

46. Giglio, L.; Csiszar, I.; Justice, C.O. Global distribution and seasonality of active fires as observed with the Terra and Aqua Moderate Resolution Imaging Spectroradiometer (MODIS) sensors. *J. Geophys. Res. Biogeosci.* **2006**, *111*, G2. [CrossRef]

47. Giglio, L.; Randerson, J.T.; Van Der Werf, G.R. Analysis of daily, monthly, and annual burned area using the fourth-generation global fire emissions database (GFED4). *J. Geophys. Res. Biogeosci.* **2013**, *118*, 317–328. [CrossRef]

48. Wotawa, G.; Novelli, P.C.; Trainer, M.; Granier, C. Inter-annual variability of summertime CO concentrations in the Northern Hemisphere explained by boreal forest fires in North America and Russia. *Geophys. Res. Lett.* **2001**, *28*, 4575–4578. [CrossRef]

49. Duncan, B.N.; Martin, R.V.; Staudt, A.C.; Yevich, R.; Logan, J.A. Interannual and seasonal variability of biomass burning emissions constrained by satellite observations. *J. Geophys. Res. Atmos.* **2003**, *108*, ACH 1-1–ACH 1-22. [CrossRef]

50. Van Der Werf, G.R.; Randerson, J.T.; Giglio, L.; Collatz, G.J.; Mu, M.; Kasibhatla, P.S.; Morton, D.C.; Defries, R.S.; Jin, Y.; Van Leeuwen, T.T. Global fire emissions and the contribution of deforestation, savanna, forest, agricultural, and peat fires (1997-2009). *Atmos. Chem. Phys.* **2010**, *10*, 11707–11735. [CrossRef]

51. Mokhov, I.I.; Chernokulsky, A.V. Regional model assessments of forest fire risks in the Asian part of Russia under climate change. *Geogr. Nat. Resour.* **2010**, *31*, 165–169. [CrossRef]

52. Ward, D.S.; Shevliakova, E.; Malyshev, S.; Rabin, S. Trends and variability of global fire emissions due to historical anthropogenic activities. *Glob. Biogeochem. Cycles* **2018**, *32*, 122–142. [CrossRef]

53. Takaya, K.; Nakamura, H. Mechanisms of intraseasonal amplification of the cold Siberian high. *J. Atmos. Sci.* **2005**, *62*, 4423–4440. [CrossRef]

54. Jiang, X.; Yang, S.; Li, Y.; Kumar, A.; Wang, W.; Gao, Z. Dynamical prediction of the East Asian winter monsoon by the NCEP climate forecast system. *J. Geophys. Res. Atmos.* **2013**, *118*, 1312–1328. [CrossRef]

55. Jiang, Z.; Worden, J.R.; Worden, H.; Deeter, M.; Jones, D.B.A.; Arellano, A.F.; Henze, D.K. A 15-year record of CO emissions constrained by MOPITT CO observations. *Atmos. Chem. Phys.* **2017**, *17*, 4565–4583. [CrossRef]

56. Han, H.; Liu, J.; Yuan, H.; Jiang, F.; Zhu, Y.; Wu, Y.; Wang, T.; Zhuang, B. Impacts of synoptic weather patterns and their persistency on free tropospheric carbon monoxide concentrations and outflow in Eastern China. *J. Geophys. Res. Atmos.* **2018**, *123*, 7024–7046. [CrossRef]

57. Kopacz, M.; Jacob, D.J.; Fisher, J.A.; Logan, J.A.; Zhang, L.; Megretskaia, I.A.; Yantosca, R.M.; Singh, K.; Henze, D.K.; Burrows, J.P.; et al. Global estimates of CO sources with high resolution by adjoint inversion of multiple satellite datasets (MOPITT, AIRS, SCIAMACHY, TES). *Atmos. Chem. Phys.* **2010**, *10*, 855–876. [CrossRef]

58. Sicard, M.; Granados-Muñoz, M.J.; Alados-Arboledas, L.; Barragán, R.; Bedoya-Velásquez, A.E.; Benavent-Oltra, J.A.; Bortoli, D.; Comerón, A.; Córdoba-Jabonero, C.; Costa, M.J.; et al. Ground/space, passive/active remote sensing observations coupled with particle dispersion modelling to understand the inter-continental transport of wildfire smoke plumes. *Remote Sens. Environ.* **2019**, *232*, 111294. [CrossRef]

59. Turquety, S.; Clerbaux, C.; Law, K.; Coheur, P.F.; Cozic, A.; Szopa, S.; Hauglustaine, D.A.; Hadji-Lazaro, J.; Gloudemans, A.M.S.; Schrijver, H.; et al. CO emission and export from Asia: An analysis combining complementary satellite measurements (MOPITT, SCIAMACHY and ACE-FTS) with global modeling. *Atmos. Chem. Phys.* **2008**, *8*, 5187–5204. [CrossRef]

60. Borsdorff, T.; Aan De Brugh, J.; Hu, H.; Hasekamp, O.; Sussmann, R.; Rettinger, M.; Hase, F.; Gross, J.; Schneider, M.; Garcia, O.; et al. Mapping carbon monoxide pollution from space down to city scales with daily global coverage. *Atmos. Meas. Tech.* **2018**, *11*, 5507–5518. [CrossRef]

61. Ribeiro, I.O.; Andreoli, R.V.; Kayano, M.T.; Sousa, T.R.; Medeiros, A.S.; Godoi, R.H.M.; Godoi, A.F.L.; Duvoisin, S.J.; Martin, S.T.; Souza, R.A.F. Biomass burning and carbon monoxide patterns in Brazil during the extreme drought years of 2005, 2010, and 2015. *Environ. Pollut.* **2018**, *243*, 1008–1014. [CrossRef]

62. Zheng, B.; Tong, D.; Li, M.; Liu, F.; Hong, C.; Geng, G.; Li, H.; Li, X.; Peng, L.; Qi, J.; et al. Trends in China's anthropogenic emissions since 2010 as the consequence of clean air actions. *Atmos. Chem. Phys.* **2018**, *18*, 14095–14111. [CrossRef]

63. Yuan, C.; Lau, W.K.M.; Li, Z.; Cribb, M. Relationship between Asian monsoon strength and transport of surface aerosols to the Asian Tropopause Aerosol Layer (ATAL): Interannual variability and decadal changes. *Atmos. Chem. Phys.* **2019**, *19*, 1901–1913. [CrossRef]

64. Van Marle, M.J.E.; Kloster, S.; Magi, B.I.; Marlon, J.R.; Daniau, A.L.; Field, R.D.; Arneth, A.; Forrest, M.; Hantson, S.; Kehrwald, N.M.; et al. Historic global biomass burning emissions for CMIP6 (BB4CMIP) based on merging satellite observations with proxies and fire models (1750-2015). *Geosci. Model Dev.* **2017**, *10*, 3329–3357. [CrossRef]

65. Bhardwaj, P.; Naja, M.; Kumar, R.; Chandola, H.C. Seasonal, interannual, and long-term variabilities in biomass burning activity over South Asia. *Environ. Sci. Pollut. Res.* **2016**, *23*, 4397–4410. [CrossRef] [PubMed]

66. Marvel, K.; Cook, B.I.; Bonfils, C.J.W.; Durack, P.J.; Smerdon, J.E.; Williams, A.P. Twentieth-century hydroclimate changes consistent with human influence. *Nature* **2019**, *569*, 59–65. [CrossRef]

67. Lian, Z.; Ouyang, W.; Hao, F.; Liu, H.; Hao, Z.; Lin, C.; He, M. Changes in fertilizer categories significantly altered the estimates of ammonia volatilizations induced from increased synthetic fertilizer application to Chinese rice fields. *Agric. Ecosyst. Environ.* **2018**, *265*, 112–122. [CrossRef]

68. Chen, W.; Li, J.; Bao, Q.; Gao, Z.; Cheng, T.; Yu, Y. Evaluation of straw open burning prohibition effect on provincial air quality during October and November 2018 in Jilin Province. *Atmosphere* **2019**, *10*, 7. [CrossRef]

69. Chen, J.; Di, X.Y. Forest fire prevention management legal regime between China and the United States. *J. For. Res.* **2015**, *26*, 447–455. [CrossRef]

70. Kukavskaya, E.A.; Buryak, L.V.; Shvetsov, E.G.; Conard, S.G.; Kalenskaya, O.P. The impact of increasing fire frequency on forest transformations in southern Siberia. *For. Ecol. Manag.* **2016**, *382*, 225–235. [CrossRef]

71. Pan, X.; Chin, M.; Ichoku, C.M.; Field, R.D. Connecting indonesian fires and drought with the type of El Niño and phase of the Indian Ocean Dipole during 1979–2016. *J. Geophys. Res. Atmos.* **2018**, *123*, 7974–7988. [CrossRef]

72. Deeter, M.N.; Emmons, L.K.; Francis, G.L.; Edwards, D.P.; Gille, J.C.; Warner, J.X.; Khattatov, B.; Ziskin, D.; Lamarque, J.F.; Ho, S.P.; et al. Operational carbon monoxide retrieval algorithm and selected results for the MOPITT instrument. *J. Geophys. Res. Atmos.* **2003**, *108*, ACH 1-1–ACH 1-11. [CrossRef]

73. Warner, J.X.; Gille, J.C.; Edwards, D.P.; Ziskin, D.C.; Smith, M.W.; Bailey, P.L.; Rokke, L. Cloud detection and clearing for the Earth Observing System Terra satellite Measurements of Pollution in the Troposphere (MOPITT) experiment. *Appl. Opt.* **2001**, *40*, 1269–1284. [CrossRef] [PubMed]

74. Deeter, M.N.; Emmons, L.K.; Edwards, D.P.; Gille, J.C.; Drummond, J.R. Vertical resolution and information content of CO profiles retrieved by MOPITT. *Geophys. Res. Lett.* **2004**, *31*, 15111–15114. [CrossRef]

75. Strow, L.L.; Hannon, S.E.; De Souza-Machado, S.; Motteler, H.E.; Tobin, D. An overview of the AIRS radiative transfer model. *IEEE Trans. Geosci. Remote Sens.* **2003**, *41*, 303–313. [CrossRef]

76. Susskind, J.; Barnet, C.D.; Blaisdell, J.M. Retrieval of atmospheric and surface parameters from AIRS/AMSU/HSB data in the presence of clouds. *IEEE Trans. Geosci. Remote Sens.* **2003**, *41*, 390–409. [CrossRef]

77. Warner, J.X.; Yang, R.; Wei, Z.; Carminati, F.; Tangborn, A.; Sun, Z.; Lahoz, W.; Attié, J.L.; El Amraoui, L.; Duncan, B. Global carbon monoxide products from combined AIRS, TES and MLS measurements on A-train satellites. *Atmos. Chem. Phys.* **2014**, *14*, 103–114. [CrossRef]